Initial mechanisms for the unimolecular decomposition of electronically excited bisfuroxan based energetic materials

Bing Yuan and Elliot R. Bernstein

Initial mechanisms for the unimolecular decomposition of electronically excited bisfuroxan based energetic materials

Bing Yuan and Elliot R. Bernstein[a)]
Department of Chemistry, Colorado State University, Fort Collins, Colorado 80523-1872, USA

Unimolecular decomposition of energetic molecules, 3,3′-diamino-4,4′-bisfuroxan (labeled as A) and 4,4′-diamino-3,3′-bisfuroxan (labeled as B), has been explored via 226/236 nm single photon laser excitation/decomposition. These two energetic molecules, subsequent to UV excitation, create NO as an initial decomposition product at the nanosecond excitation energies (5.0–5.5 eV) with warm vibrational temperature (1170 ± 50 K for A, 1400 ± 50 K for B) and cold rotational temperature (<55 K). Initial decomposition mechanisms for these two electronically excited, isolated molecules are explored at the complete active space self-consistent field (CASSCF(12,12)/6-31G(d)) level with and without MP2 correction. Potential energy surface calculations illustrate that conical intersections play an essential role in the calculated decomposition mechanisms. Based on experimental observations and theoretical calculations, NO product is released through opening of the furoxan ring: ring opening can occur either on the S_1 excited or S_0 ground electronic state. The reaction path with the lowest energetic barrier is that for which the furoxan ring opens on the S_1 state via the breaking of the N1—O1 bond. Subsequently, the molecule moves to the ground S_0 state through related ring-opening conical intersections, and an NO product is formed on the ground state surface with little rotational excitation at the last NO dissociation step. For the ground state ring opening decomposition mechanism, the N—O bond and C—N bond break together in order to generate dissociated NO. With the MP2 correction for the CASSCF(12,12) surface, the potential energies of molecules with dissociated NO product are in the range from 2.04 to 3.14 eV, close to the theoretical result for the density functional theory (B3LYP) and MP2 methods. The CASMP2(12,12) corrected approach is essential in order to obtain a reasonable potential energy surface that corresponds to the observed decomposition behavior of these molecules. Apparently, highly excited states are essential for an accurate representation of the kinetics and dynamics of excited state decomposition of both of these bisfuroxan energetic molecules. The experimental vibrational temperatures of NO products of A and B are about 800–1000 K lower than previously studied energetic molecules with NO as a decomposition product. *Published by AIP Publishing.* [http://dx.doi.org/10.1063/1.4972259]

I. INTRODUCTION

Heterocycle-based energetic compounds, such as triazole, tetrazole, tetrazine, furazan, and furoxan derivatives, are reported and extensively applied as high-energy explosives and ingredients of propellants because of their good energetic performance, high nitrogen content, and good thermal stability.[1] The furoxan ring, containing an active oxygen atom in the ring, which forms a veiled nitro group in combination with an N-oxide fragment, is a useful building block in the synthesis of energetic materials with nitrogen containing heterocycles.[1,2]

The structure of furoxan ring is shown in Figure 1; it is characterized as an electron rich system, with a pronounced withdrawal of electronic charge by the O atom of the N-oxide moiety (exocyclic O atom).[3–5] The N—O bond of the exocyclic N—oxide moiety is reported to be as short as an actual double bond, while the endocyclic N—O bond is longer than a typical single bond for this moiety.[3] The chemical

structure of furoxan suggests that it can be a potential NO generator through decomposition with the breaking of the endocyclic N—O bond.[6–9] In the study of diaminofuroxan, the most favorable decomposition process is ring opening via the endocyclic N—O bond closer to the N-oxide group: this bond breaking requires 94.62 kJ/mol of energy. Ring opening via the other endocyclic N—O bond requires ~120 kJ/mol of energy.[2]

This report deals specifically with the unimolecular decomposition of the energetic materials, 3,3′-diamino-4,4′-bisfuroxan (labeled as A) and 4,4′-diamino-3,3′-bisfuroxan (labeled as B): their structures are shown in Figure 1. Both A and B have two furoxan rings connected through their ring C atoms, forming a C—C bridge with one amino functional group on each furoxan ring substituted for the H atom on the other C atom of the same ring. From previous studies, the furoxan rings as well as the amine nitrogen atoms of A form a plane, while in B the rings are twisted by 48°.[10] The crystal of A forms a network of intermolecular hydrogen bonds between the amine groups and the exocyclic O atoms.[10] Hydrogen bonding for the crystal of B consists of intramolecular hydrogen bonds between the exocyclic O atom on one furoxan ring with the

---

a)Author to whom correspondence should be addressed. Electronic mail: erb@Colostate.edu

146, 014301-1

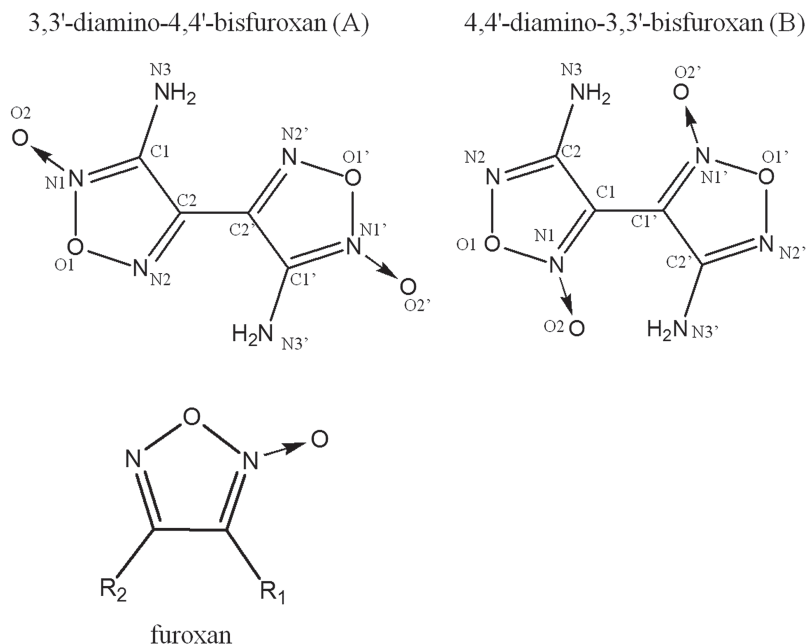3,3'-diamino-4,4'-bisfuroxan (A)   4,4'-diamino-3,3'-bisfuroxan (B)

FIG. 1. Chemical structures of 3,3′-diamino-4,4′-bisfuroxan (A) and 4,4′-diamino-3,3′-bisfuroxan (B) with numbering for all the atoms.

NH_2 on the other furoxan ring, in addition to the intermolecular hydrogen bonds characterized for the A crystal.[10] In the synthesis process, structure A is the kinetically favored product, while B is the thermodynamically favored product. Structure A starts to decompose at 160 °C and the decomposition temperature of B is 170 °C.[10] The impact sensitivity of A and B is 6 J and 10 J, respectively. The impact sensitivity of RDX equals 7.5 J: B is less impact sensitive than RDX.[10] The friction sensitivity of both A and B is greater than 360 N, a lot better than that for RDX, which equals 120 N.[10] Both A and B show good detonation velocities (A is 9007 m/s, B is 8740 m/s), which are comparable to or even higher than that reported for RDX (8855 m/s).[10]

In addition to the study of sensitivity, heat of formation, and denotation velocity for condensed phase energetic materials, the study of the initial bond dissociation reactions and decomposition mechanisms for the unimolecular chemistry that initiates the release of stored energy from energetic materials also provides crucial information concerning energetic properties.[11,12] A particularly essential application of this latter fundamental detail concerning energetic materials is for the design of new energetic species and chemical classes.[13,14] This molecular approach emphasizes isolated energetic molecule behavior as the central first step in the energy release processes in either gas or condensed phase.[13–16] The assumed methodology can be justified by the local nature of the molecular excitation processes that occur upon even gentle shock wave excitation in any organic molecular solid, as discussed below. Thus, focus of the present effort is the decomposition of isolated, electronically excited, energetic molecules, diamino-bisfuroxans A and B, both experimentally and theoretically. The initial decomposition product molecule or species is observed and characterized, and decomposition mechanisms are calculated for a single energetic species theoretically: this approach to the elucidation of reaction kinetics/dynamics/mechanism has been pursued for many decades.[11–17]

In general, the difference between condensed phase and gas phase reactions is that solid state reactions occur within the rigid constraining environment of a crystal lattice, in which intermolecular interactions can influence reaction mechanisms and directions.[18] Other important factors that can affect the solid reactions include the presence of solvates, planar defects, phase transitions, disorder, and even crystal morphology.[18] Although condensed phase reactions can be more complicated than gas phase ones, studies of the unimolecular behavior of explosives enable researchers to understand initial decomposition mechanisms; moreover, the revealed mechanisms provide useful understanding and insight into the design of new energetic materials.[11,17]

Energetic materials are sensitive to stored energy release initiation by heat, electrostatic discharge, impact, friction, shock, and laser irradiation.[19] The initiation of detonation is often considered to be associated with the formation of crystal hot spots, which are small regions of the crystal localizing some portion of the energy introduced by an external stimulus.[15,19] If enough hot spot energy is stored in lattice, it will be channeled into appropriate molecular vibration modes: such energy localization can cause bond scission and/or other events that lead to self-sustaining exothermic chemical decomposition.[15,19] Certain types of molecular bonds are particularly susceptible to rupture by the input of hot spot energy and these are readily identified and elucidated by the present isolated, single molecule strategies.[13–15]

In our studies, we have followed decomposition mechanisms for various classes of energetic materials initiated from excited electronic states. Based on the centuries old observations of triboluminescence, one readily concludes that molecular electronic excitation must contribute to the initial chemical reactions that begin the release of stored molecular energy for an energetic system.[20–26] Isolated molecule experiments and theory represent a reasonable approximation to the primary, initial behavior for the decomposition of energetic molecules in general condensed phase

materials. Based on the experimental results, theoretical calculations are applied in order to explicate experimental data and to construct appropriate decomposition mechanisms. Nonadiabatic interactions through conical intersections between zero order adiabatic electronic states play a key role in the ultrafast (<100 fs) decomposition pathways proffered.[27–32] Determination of decomposition reaction kinetics, dynamics, and mechanisms for these large energetic molecules energized to excited electronic states (by shocks, arcs, sparks, light, . . .) emphasizes the importance of fundamental chemical physics to the technological advance of newly synthesized molecular energy storage systems, energetic materials, and fuels. The capacity of computational chemistry to assist in the design, characterization, and evaluation of compounds of real practical importance has greatly increased during the past ten years.[13,14,18]

In the present report, energy resolved spectra of the initial product molecule NO, fragmented from electronically excited bisfuroxans, are studied to define the decomposition kinetics and dynamics of the energetic material isolated molecules. These spectra facilitate the characterization of the decomposition processes through elucidation of the rotational and vibrational temperatures of the ground electronic state NO product. Potential energy surfaces for the excited and ground electronic states of A and B are explored theoretically, employing quantum chemistry calculations (Gaussian 09—complete active space self-consistent field (CASSCF), density functional theory (DFT), MP2, CASSCFMP2). Detailed decomposition mechanisms for 3,3′-diamino-4,4′-bisfuroxan (A) and 4,4′-diamino-3,3′-bisfuroxan (B) are thereby proposed and discussed. Furoxan ring opening decomposition mechanisms are calculated and the energy barriers for the ring opening via the C—N bond and N—O bond are compared. Ring opening processes on the first excited singlet electronic state and ground state surfaces are both explored. A detailed explication of the decomposition mechanisms for these energetic species is provided. In order to generate the most reasonable decomposition potential surface, different quantum chemistry calculational methods are applied, including DFT, MP2, CASSCF (different electrons and orbitals are chosen), and CASMP2. CASMP2 is an MP2-level electron correlation correction to the CASSCF energy computed during a CASSCF calculation.[33–35] These studies are both fundamental and practical as they make advances toward the application of fundamental chemical physics specifically to the behavior of new organic molecular, energy storage materials.

II. EXPERIMENTAL PROCEDURES

The experimental setup consists of a matrix-assisted laser desorption (MALD) system, a supersonic jet expansion nozzle, and a time-of-flight mass spectrometer. Details of the instrumental design are described in our previous papers.[28,29] The nozzle used for the molecular beam generation is constructed from a Jordan Co. pulsed valve and a laser ablation attachment. The nonvolatile samples are desorbed from the drum by 532 nm ablation laser, entrained in the flow of He carried gas under a pressure of 80 psi through the 2×60 mm

channel in the laser desorption head, and expanded into the vacuum chamber. With 80 psi He backing pressure for the closed pulsed valve, the chamber pressure remains 2×10^{-7} Torr; with the valve open at 10 Hz, the chamber pressure increases to 4×10^{-7} Torr.

All sample drums for MALD are prepared by wrapping a piece of porous filter paper around a clean Al drum. A solution of 0.02 mol/l matrix (R6G) and 0.01 mol/l sample in methanol is uniformly sprayed on the drum surface while it is rotating under a halogen heat lamp in a fume hood to make sure the sample coating is dry. Rhodamine 6G is chosen because it has an intense absorption at 532 nm; consequently, it can efficiently absorb the 532 nm laser photons and decompose. This process expels the intact energetic molecules, trapped in the dye matrix, into the supersonic expansion gas flow from the pulsed nozzle. Both bisfuroxan samples were supplied by Professor Thomas M. Klapökte, Ludwig-Maximilian University of Munich.

In addition to ablation laser, one or two others laser are required to photoexcite the sample in the beam and then detect the photo-dissociated fragments. Laser ablation of any molecule will generate both ionic and neutral species. In our apparatus, only the neutrals can enter the electric field extraction/ionization region because the plates are continuously charged to 4.0 kV and 3.75 kV, as is usual for a linear 1 m time of flight mass spectrometer with a 3 plate ion focusing region for laser ionization of neutrals.

For NO detection, a single pump/probe laser is used at 226 and 236 nm for both initiation of energetic sample and detection of the NO product following a one color (1+1) resonance-enhanced two photon ionization (R2PI) scheme [A(v′ = 0) ← X(v″ = 0–1) and I ← A transitions] through TOFMS.[36] The proper UV laser wavelengths for this process are generated by a dye laser, pumped by the second harmonic (532 nm) of a Nd: yttrium aluminum garnet laser's fundamental output (1.064 μm), in conjunction with a wavelength extension system. The typical pulse energy of the UV laser is ∼200 μJ/pulse, which gives an intensity of ∼6.0 × 10^7 W/cm^2 for a 8 ns pulse duration. The spectra are not saturated and only single photon absorption occurs for the sample and the NO product at ca. 50 μJ/pulse between 236 and 226 nm. The molecular beam is perpendicularly crossed by the UV laser beam, which is focused to a spot size of about 0.2 mm diameter at the ionization region of the TOFMS.

The timing sequence of pulsed nozzle, ablation laser, and excitation/ionization laser are controlled by time delay generators (SRS DG535). The experiment is run at a repetition rate of 10 Hz. Ion signals in the TOFMS are detected by a microchannel plate (MCP) and signals are recorded and processed on a personal computer (PC) using an analog-to-digital converter (ADC) card (Analog Devices RTI-800) and a boxcar averager (SRS SR 250).

Since no experimental data exist for vertical excitation energies of the two diamino-bisfuroxan molecules, in order to determine the accuracy of theoretical calculation for the energies of higher electronic states, the experimental UV-Vis absorption spectra of these two energetic materials are taken with an UV-Vis-NIR Varian Cary 500 spectrometer in the range from 200 nm to 800 nm. The two samples are dissolved in

methanol with concentrations between 10^{-6} and 10^{-5} mol/l. These spectra are discussed in Section IV.

III. COMPUTATIONAL METHODS

All calculations are executed at the CASSCF(12,12)/6-31G(d), CASMP2(12,12)/6-31G(d), and B3LYP/6-31G(d) levels of theory with the Gaussian 09 program. No symmetry restrictions are applied for the calculations. Equilibrium geometry calculations are conducted taking the total charge as neutral and the spin multiplicity as 1. To explore the excited state potential energy surfaces, the active space comprises 12 electrons distributed in 12 orbitals, denoted as CASSCF (12,12). The chosen orbitals are molecular orbitals from HOMO−5 to LUMO+5 (Fig. 2). Molecular structures and energies in CASSCF(12,12), CASMP2(12,12), and B3LYP methods with basis set 6-31G(d) are compared in order to find the most reasonable potential surfaces for the decomposition. Excitation energies are calculated by state averaging over the ground and excited states with equal weights for each state. Larger basis

sets than 6-31G(d) for these CASSCF calculations do not substantially improve the results and understanding of the reaction mechanisms.[37,38]

Critical points (minimum, transition state, and conical intersection structures) are characterized by analytical frequency calculations, and minimum energy paths are calculated using an intrinsic reaction coordinate (IRC) algorithm implemented in the Gaussian 09 program suite. The maximum orbital limit for the CASSCF method for conical intersection and transition state calculations is eight due to the need for analytic second derivatives; therefore, for these two critical point calculations, a CASSCF(12,8) is applied initially in order to obtain optimized geometric structures. Then CASSCF(12,12) is employed as a single point calculation based on the structure of CASSCF(12,8) for more accurate potential energies.

To find the minimum and most reasonable decomposition pathways, a relaxed scan optimization algorithm as implemented is employed in which all geometrical parameters except for the specified bond distance are optimized
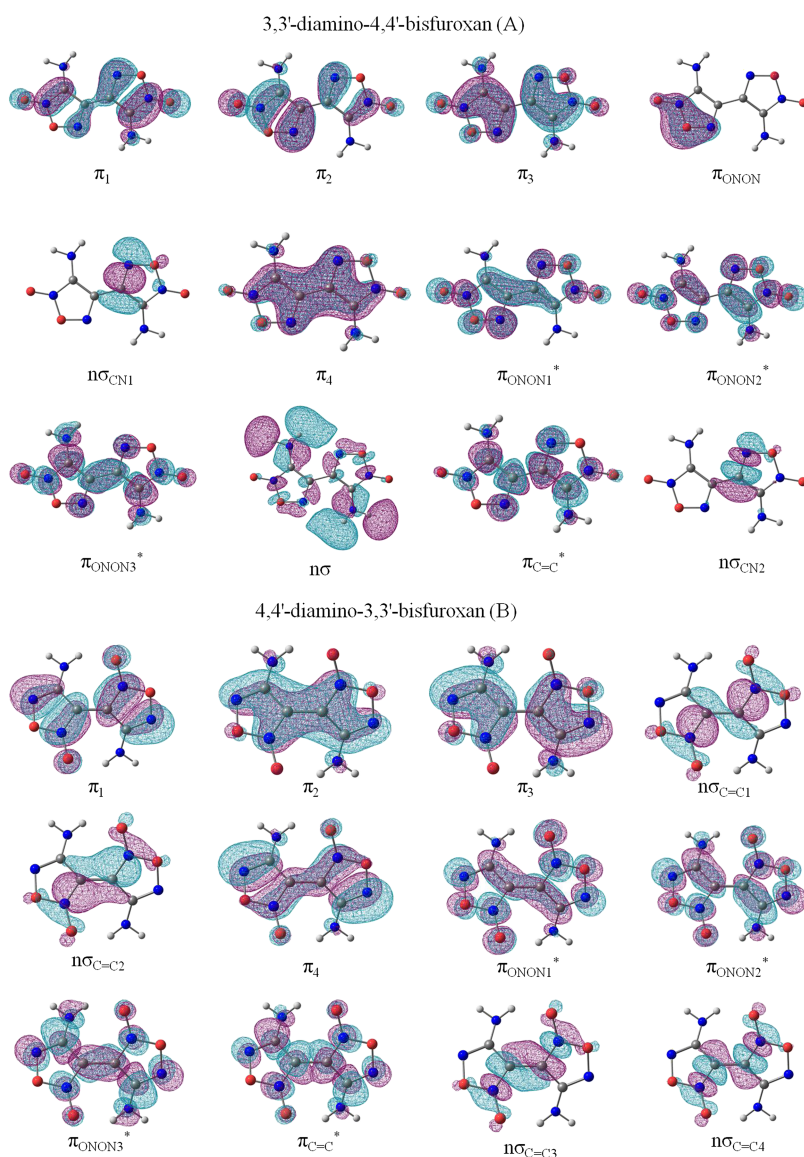

FIG. 2. (a) Orbitals used in the active space of CASSCF calculations for 3,3′-diamino-4,4′-bisfuroxan (A). The (12,12) active space comprises four π-bonding orbitals over the whole system π_1, π_2, π_3, and π_4, one π-bonding orbital on the O−N−O−N moiety π_{ONON}, two nonbonding orbitals around the C−N bond $n\sigma_{CN1}$ and $n\sigma_{CN2}$, three π-antibonding orbitals around the O−N−O−N moiety π_{ONON1}^*, π_{ONON2}^*, and π_{ONON3}^*, one π-antibonding orbital around the C=C bond $\pi_{C=C}^*$, and one σ-nonbonding delocalized orbital $n\sigma$ around the whole system. For atoms in the structure, grey is carbon, blue is nitrogen, red is oxygen, and white is hydrogen. (b) Orbitals used in the active space of CASSCF calculations for 4,4′-diamino-3,3′-bisfuroxane (B). The (12,12) active space comprises four π-bonding orbitals over the whole system π_1, π_2, π_3, and π_4, four nonbonding orbitals around the C=C bond $n\sigma_{C=C1}$, $n\sigma_{C=C2}$, $n\sigma_{C=C3}$, and $n\sigma_{C=C4}$, three π-antibonding orbitals around the O−N−O−N moiety π_{ONON1}^*, π_{ONON2}^*, and π_{ONON3}^*, and one π-antibonding orbital around the C=C bond $\pi_{C=C}^*$. For atoms in the structure, grey is carbon, blue is nitrogen, red is oxygen, and white is hydrogen.

and electronic energies are monitored as the specified bond is elongated. The bond length increase for each step is 0.1 Å for a total scan length of 3.0–4.0 Å. In the scan of NO dissociation from the molecular system, different CASSCF levels, including CASSCF(6,5), CASSCF(10,9), CASSCF(8,14), CASSCF(12,12), and CASMP2(12,12), as well as B3LYP and MP2 methods with basis set 6-31G(d), are all applied and compared. As will be demonstrated and discussed below, the exploration of such extensive and comprehensive CASSCF based calculations for generation of appropriate potential energy surfaces for these systems is unusual, but is required to obtain accurate and converged reaction surfaces essential to derive mechanisms that comport with the experimental findings. These bisfuroxans require a significant inclusion of highly excited electronic states in order to describe their non-Born Oppenheimer, non-adiabatic chemical behavior: both MP2 and DFT approaches provide approximations to the multi-reference configuration interaction necessary to describe this chemistry.

The accuracies of the calculations along the reaction pathway are difficult to estimate and establish since the experimental information about conical intersections and transition states is not at present available. Calculations presented in this paper, however, are based on the experimental observations including decomposition products and the internal energy distributions within these products. Therefore, the proposed reaction pathways based on the computational results provide a reasonable and, at minimum qualitative, interpretation of the experimental observations.

IV. EXPERIMENTAL RESULTS AND DISCUSSION

A. UV-Vis absorption spectra of bisfuroxan

The UV-Vis absorption spectra for the two diamino-bisfuroxans A and B are shown in Figure 3: the maximum absorption wavelengths in the experimental range for A are 350 and 238 nm, and for B, are 325 (weak and broad), 282, and 242 nm. The maximum absorption wavelengths of these two bisfuroxan molecules are comparable to each other and the differences are most likely caused by the extra intramolecular hydrogen bonds in B between an H atom of the NH$_2$ group and the O atom in the nearby N-oxide moiety of the other furoxan ring. For the decomposition study, the laser wavelength is set to 226 or 236 nm. Excitation and decomposition of these two energetic molecules occurs through single photon absorption. As NO detection is a one color, (1+1), resonance-enhanced, two photon ionization (REMPI) process, totally three photons are involved in the overall decomposition/NO detection of molecules A and B.

B. Decomposition product NO

The NO product is observed as a major decomposition product from both electronically excited A and B at 226 and 236 nm by TOFMS. The 226/236 nm excitation wavelength corresponds to the resonance (0–0)/(0–1) vibronic bands for $A^2\Sigma^+ \leftarrow X^2\Pi$ electronic transition of the NO product. The 248 nm excitation wavelength corresponding to the resonance (0–2) vibronic bands of the NO product is also employed in the decomposition; however, the NO signal is too weak to be observed at this transition. By scanning the laser excitation wavelengths, (1+1) R2PI rotationally resolved spectra of the NO product from A and B molecules are obtained. The linewidth of the NO mass peak is 10 ns (the laser pulse width), consistent with that expected for decomposition from the lowest few excited states. Thus, the NO product is associated with single photon absorption for these two energetic molecules. Hot diamino-bisfuroxans, which might be generated in the ablation process, are effectively relaxed and cooled in the highly collisional supersonic expansion process through the nozzle.

Figures 4 and 5 show the spectra of two different $A(v' = 0) \leftarrow X(v'' = 0,1)$ rovibronic transitions of the NO molecule generated from A and B excited to their first excited electronic states. All spectra have similar rotational patterns but a different vibrational intensity for each vibronic band. The most intense rotational feature in each spectrum of NO
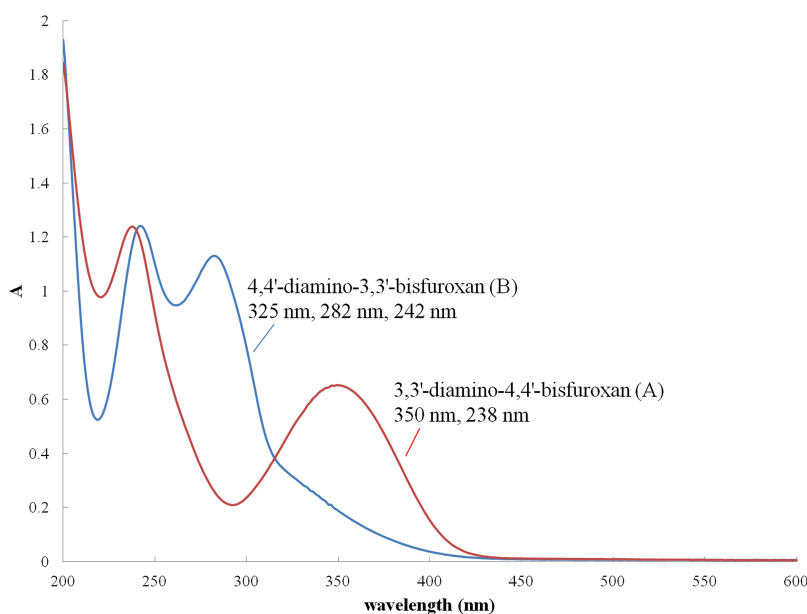

FIG. 3. UV-Vis absorption spectra of 3,3′-diamino-4,4′-bisfuroxan (A) and 4,4′-diamino-3,3′-bisfuroxan (B) with maximum absorption wavelengths. Both samples are dissolved in methanol with concentration <10^{-5} mol/l.

4,4'-diamino-3,3'-bisfuroxan (B)
325 nm, 282 nm, 242 nm

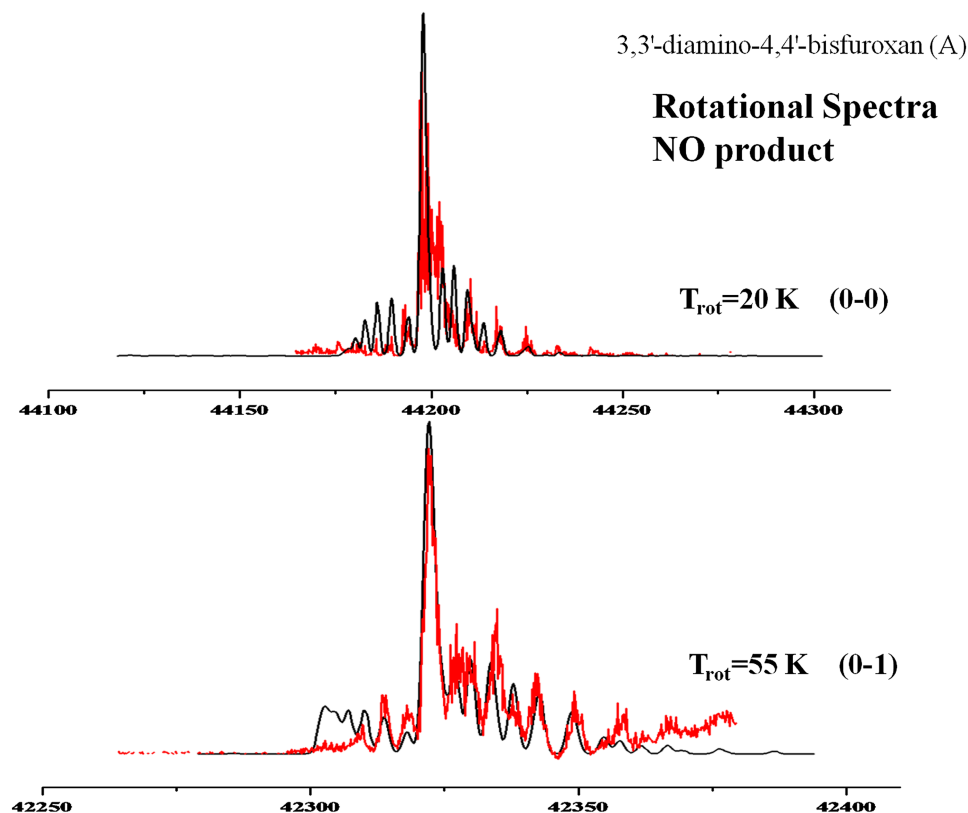3,3'-diamino-4,4'-bisfuroxan (A)
350 nm, 238 nm

FIG. 4. One color (1+1) R2PI spectra of the vibronic transitions $A^2\Sigma^+(v' = 0) \leftarrow X^2\Pi(v'' = 0, 1)$ of the NO product from the excited electronic state decomposition of 3,3'-diamino-4,4'-bisfuroxan (A). Rotational simulations with a Boltzmann population distribution show that the rotational temperatures are 20 K and 55 K, respectively, for the two observed vibrational levels (0–0) and (0–1) of the ground electronic state with ±10 K uncertainty. The black line is the experimental data and the red one is the simulation for the NO (A–X) transition.

corresponds to the $(Q_{11} + P_{12})$ band, and the lower intensity features for each vibronic transition correspond to other rotational transitions.[36] The rotational temperatures of the two

vibrational levels $(v'' = 0, 1)$ in the ground electronic state of NO product from the two diamino-bisfuroxan molecules can be obtained through the spectral simulations based on
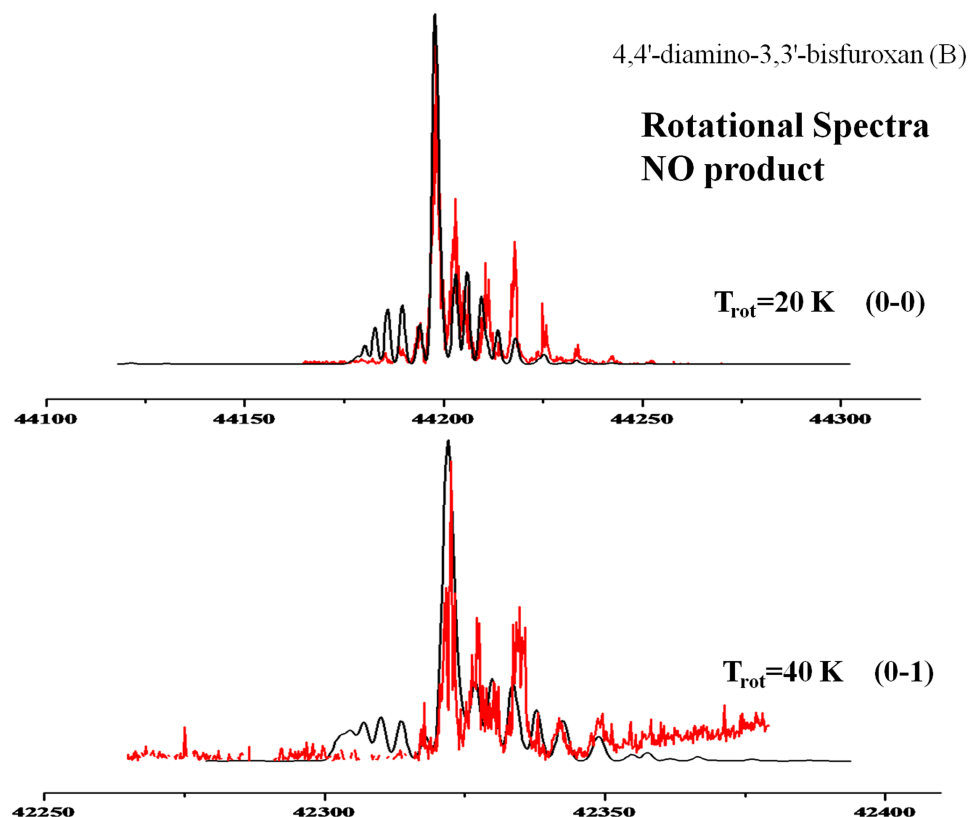

FIG. 5. One color (1+1) R2PI spectra of the vibronic transitions $A^2\Sigma^+(v' = 0) \leftarrow X^2\Pi(v'' = 0, 1)$ of the NO product from the excited electronic state decomposition of 4,4'-diamino-3,3'-bisfuroxan (B). Rotational simulations with a Boltzmann population distribution show that the rotational temperatures are 20 K and 40 K, respectively, for the two observed vibrational levels (0–0) and (0–1) of the ground electronic state with ±10 K uncertainty. The black line is the experimental data and the red one is the simulation for the NO (A–X) transition.

Boltzmann population distributions. The vibrational temperature of the NO product can be obtained by simulating the relative intensities among the observed vibronic bands, using a Boltzmann population distribution analysis and Franck-Condon factors. The Franck-Condon factors are calculated using the program, Lifbase: Data Base and Spectra Simulation (version 2.1.1). Details of rotational and vibrational temperature calculations are presented in our previous work.[39] The simulated rotational temperatures for A and B are similar and increase from (20 ± 10) K to (55 ± 10) K as the vibronic bands change from the (0–0) to (0–1) transition. The vibrational temperatures of NO from the two diamino-bisfuroxan molecules are calculated to be (1170 ± 50) K for A and (1400 ± 50) K for B. The experimental vibrational temperatures of NO products from both energetic molecules are about 800–1000 K lower compared to the previously characterized energetic molecules with NO as a decomposition product; for example DNP, FOX-7, and TKX-50.[38–40] The $A(v' = 0) \leftarrow X(v'' = 2)$ transition of NO product, potentially observed at 248 nm wavelength, is not detected for either molecule A or B.

In summary, the NO product from electronically excited dianimo-bisfuroxans has low rotational and warm vibrational temperatures. The vibrational temperatures of NO product will be discussed in more detail in Section V, through quantum chemistry calculations.

Even though the MALD technique is known to desorb fragile molecules in the gas phase with little if any fragmentation, the observed NO product is proven to be created in the excitation/ionization region of our instrument in three ways in our previous study.[28] Nonetheless, the NO product can also be produced from NO_2 fragmentation of A and B molecules, as well. In our previous study of NO_2 photolysis, however, the rotational temperature of NO product from an NO_2 supersonic beam is ~130 K for the $A(v' = 0) \leftarrow X(v'' = 0)$ vibronic transition and ~400 K for the $A(v' = 0) \leftarrow X(v'' = 1)$ vibronic transition.[41–43] As the rotational temperatures of the NO product from diamino-bisfuroxans are much lower than that for NO_2 photolysis, NO_2 is not the precursor for the NO product, and NO_2 loss is not the major reaction channel for the decomposition of electronically excited A and B. For molecules in which an NO_2 moiety is present, NO is generated through a mechanism involving a nitro-nitrite isomerization in the intact, electronically excited, parent molecule: rupture of a ring N—O bond of either A or B should also follow such a reaction pathway, even in an intermediate or transition state species.[27,37–44]

V. THEORETICAL RESULTS AND DISCUSSION

A. Structures of diamino-bisfuroxan A and B and their excitation energies

The ground state structures of the two diamino-bisfuroxan molecules A and B are calculated at both B3LYP/6-31G(d) and CASSCF(12,12)/6-31G(d) levels. Based on the previous X-ray diffraction result for A, the furoxan ring as well as the amine group nitrogen atoms is coplanar, while for B, the furoxan rings are twisted by 48°.[10] In our theoretical calculation of gas phase isolated molecules, structure A has a torsion dihedral

angle C1—C2—C2′—C1′ (labels in Figure 1) of −169.922° and −176.775° from CASSCF(12,12) and B3LYP methods, respectively. The two furoxan rings of A are twisted by 10.1° within the CASSCF and by 3.3° within B3LYP methods. The dihedral angles N3—C1—C2—C2′ and N3—C1—O1—N2 are 8.158° and 168.274° within the CASSCF method, and within the B3LYP method they equal to 6.315° and 170.236°, respectively. Based on these dihedral angles, the two furoxan rings and the nitrogen atoms of the amine groups are nearly planar with a twist smaller than 15°. Structure B has a torsion dihedral angle C2—C1—C1′—C2′ (labels in Figure 1) of −144.625° and 145.885° within the CASSCF(12, 12) and B3LYP methods, respectively: the two furoxan rings are thus twisted by 35.4° within the CASSCF and by 34.1° within the B3LYP method. The dihedral angles N3—C2—C1—C1′ and N3—C2—N2—O1 are 8.15° and 168.274° within the CASSCF method, and within the B3LYP method they equal 3.159° and 167.8°, respectively. Compared to structure A, the two furoxan rings of B have a larger non-planar twist, as is consistent with previous studies.[10] The nitrogen atoms of the NH_2 groups for B are nearly planar with their respective to furoxan rings, which is similar to the situation for A. Detailed structural data for diamino-bisfuroxan molecules has not been previously published; thus, we summarize and compare the optimized geometries of A and B with that of a single furoxan ring and its phenyl derivative in Table I. From the CASSCF(12,12) method, the C—C bonds of the bisfuroxan rings in A and B are 1.426 and 1.443 Å, respectively, shorter than the typical C—C single bond (1.54 Å).[45] The C—N bonds in the bisfuroxan rings of A and B are in the range from 1.29 to 1.33 Å: this range is between a C—N single bond (1.47 Å) and a C=N double bond (1.22 Å).[45] The exocyclic N1—O2 bonds (labels in Figure 1) are 1.234 and 1.231 Å in A and B structures, respectively, and are consistent with previous studies.[3] Note that the N—O exocyclic bond of the furoxan N-oxide moiety is as short as an actual double bond. The endocyclic N—O bonds N1—O1 and N2—O1 of A and B molecules are 1.33–1.37 Å, about 0.1 Å longer than the N1—O2 exocyclic bond. The B3LYP method shows similar results compared to those of the CASSCF(12,12) calculation (bond length differences <0.03 Å and the bond angle differences <3.0°), except for the endocyclic N1—O1 bonds, which lie between 1.41 and 1.47 Å, about a 0.1 Å longer compared to the CASSCF values. Using the CASSCF(12,12) method, the two N—O endocyclic bonds have both single and double bond characters. In the B3LYP method, one of the endocyclic bonds N2—O1 has both single and double characters, and the other endocyclic bond N1—O1 is closer to a single bond. This geometric difference might cause some differences in decomposition mechanisms, which will be discussed in Sections V B and V C. These diamino-bisfuroxan theoretical ring structures are close to those for a single furoxan molecule and its derivative (Table I), in which C—C and C—N bonds lie between single and double bonds, exocyclic N—O bond is a double bond in the range 1.20–1.23 Å, and endocyclic N—O bonds are in the range 1.36–1.44 Å.

Experimental results yield that the NO molecule is the initial nanosecond electronic excitation decomposition product for the diamino-bisfuroxan system explored under this

TABLE I. Comparison of diamino-bisfuroxan structural parameters with furoxan and a derivative. Labels of the atoms are shown in Figure 1. Bond lengths are in angstroms and angles are in degrees.

	A		B		Furoxan[a]	3-phenylfuroxan[b]
	CASSCF (12, 12)	B3LYP	CASSCF (12, 12)	B3LYP		
C—C	1.426 58	1.421 73	1.443 20	1.437 84	1.407	1.417
C2—N2	1.297 74	1.318 69	1.292 75	1.316 57	1.273	1.293
N2—O1	1.337 45	1.353 56	1.368 21	1.389 24	1.383	1.366
N1—O1	1.359 43	1.476 92	1.336 32	1.411 04	1.377	1.436
C1—N1	1.307 43	1.330 04	1.321 53	1.337 88	1.301	1.320
N1—O2	1.234 16	1.231 51	1.235 02	1.235 96	1.203	1.235
C2—C1—N1	104.722	106.767	104.842	105.932	107.0	104.9
C1—N1—O1	109.283	106.339	109.444	108.042	108.1	108.2
N1—O1—N2	109.087	107.826	109.430	108.567	107.2	107.4
O1—N2—C2	107.190	107.595	107.063	106.611	105.1	106.6
N2—C2—C1	109.704	111.470	109.208	110.816	110.7	112.8
C1—N1—O2	131.419	133.156	131.707	133.536	134.7	135.4

[a]Reference 5.
[b]Reference 6.

study. In order to understand the experimental data more completely and derive reaction mechanisms, the theoretical calculations of molecular geometries and energies for the Franck-Condon structures, conical intersections, transition states, and intermediate states along both the ground and excited state potential energy surfaces are explored for both A and B. These theoretically derived reaction paths with potential energies and molecular geometries are shown in Figures 6, 7, 12, and 13. All these reaction channels are considered because they are energy accessible for the creation of an NO product.

Calculations at the CASSCF(12,12)/6-31G(d), CASMP2 (12,12)/6-31G(d), and TD-DFT/6-31G(d) levels are employed to determine the vertical excitation energies for diamino-bisfuroxans A and B from the ground electronic state S_0 (FC structure) to the first and second excited states S_1 and S_2. The vertical excitations calculated for the S_1 and S_2 electronic states of A are 3.57 and 4.73 eV within the CASSCF(12,12) method, 3.11 and 3.49 eV within the CASMP2(12,12) method, and they equal 3.31 and 3.38 eV in TD-DFT method. The maximum absorption wavelengths of A in UV-Vis absorption spectra shown in Figure 3 are 350 nm (3.54 eV) and 238 nm (5.20 eV). CASSCF(12,12) provides the closest theoretical result to the absorption spectra with deviation less than 0.5 eV. The absorption peak at 350 nm is much broader than the peak at 238 nm, and thus the strong absorption at 350 nm might be a combination of several absorption bands: in this case, results of the CASMP2 and B3LYP calculations, with S_1 and S_2 excitation energies between 3.11 eV and 3.38 eV, are also reasonable. Based on the available information, which method is more reasonable is not clear.

Vertical excitations calculated for the S_1 and S_2 electronic states of B are 3.29 and 4.27 eV within the CASSCF(12,12) method, 4.04 and 5.75 eV within the CASMP2(12,12) method, and 3.82 and 3.86 eV within the TD-DFT method. The three absorption wavelengths of B in UV-Vis absorption spectra shown in Figure 3 are 325 nm (3.81 eV), 282 nm (4.40 eV), and 242 nm (5.12 eV). Compared to the absorption spectra,

CASMP2 provides the most accurate excitation energies for B with errors within ~0.5 eV, which is acceptable for the current CASSCF calculations.[46,47]

Additionally, for the decomposition mechanisms of both A and B, only molecular singlet states and singlet-singlet transitions are considered, because based on our previous femtosecond studies of energetic molecules RDX and HMX, the decomposition dynamics fall into the time scale of our excitation pulse duration (ca. 100 fs).[29] These results emphasize that gas phase energetic material decomposition is an extremely fast non-adiabatic reaction at the molecular level. Molecular singlet-singlet transitions are much faster than singlet-triplet, spin forbidden transitions. The time scale of molecular fluorescence emission is between 10^{-7} and 10^{-10} s, while that for phosphorescence emission is 10^{-5} s to 10 s.[48] Therefore, singlet-triplet transitions and couplings are not the initial, main energy release mechanisms for these energetic systems.

B. Potential energy surfaces for 3,3′-diamino-4, 4′- bisfuroxan (A)

Schematic one-dimensional projections of the multidimensional singlet potential energy surfaces (S_0 and S_1) of 3,3′-diamino-4,4′-bisfuroxan (A), with locations and potential energies (the presented energies are not corrected for zero point energy) for different critical points and conical intersections along several energy available reaction paths, are plotted in Figure 6. The structures of critical points and conical intersections for A are summarized in Figure 7. The reaction coordinates depicted in Figure 6 include C—N and N—O bond lengths within the furoxan rings, either of which can be an active site for the fragmentation of molecule A: red, orange, purple, and blue arrows in Figure 6 indicate different possible decomposition channels. In Figures 6 and 7, FC geometry $S_{0,FC}$ is the optimized minimum energy of A for the S_0 state, and $(S_1/S_0)_{CI(1)-(3)}$ are conical intersections between the S_0 and S_1 states. $S_{1,TS}$ is the excited transition
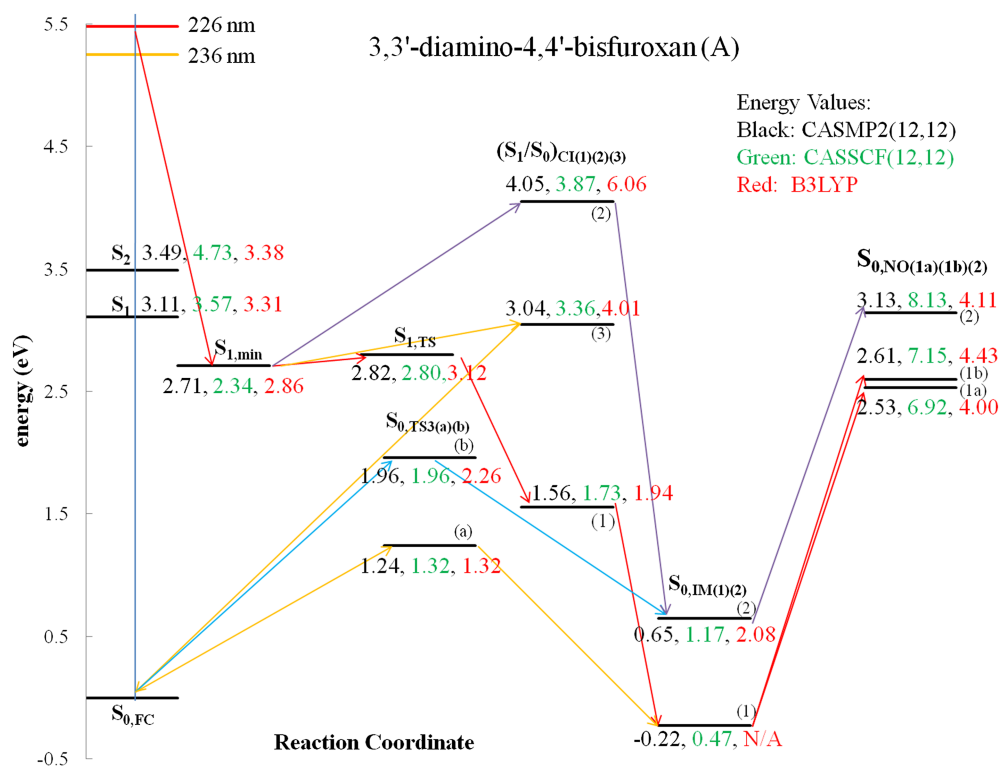
FIG. 6. A schematic one-dimensional projection of the multi-dimensional energy surfaces for 3,3′-diamino-4,4′-bisfuroxan (A) dissociation paths computed at the CASSCF(12,12)/6-31G(d), CASMP2(12,12)/6-31G(d), and TD-DFT(DFT)/6-31G(d) levels of theory. The diagram is plotted based on the potential energies from CASMP2 corrected level and the potential energies of each critical point are labeled: values in black are potential energies calculated via CASMP2(12,12)/6-31G(d), green numbers are calculated via CASSCF(12,12)/6-31G(d) without an MP2 correction, and red numbers are calculated via B3LYP/6-31G(d) and TD-DFT/6-31G(d). The red, orange, purple, and blue arrows represent different reaction channels for NO dissociation. FC geometry $S_{0,FC}$ is the optimized minimum energy of A for the S_0 state, and $(S_1/S_0)_{CI(1)-(3)}$ are conical intersections between the S_0 and S_1 states. Along pathways (1) and (2), the furoxan ring opens through the N—O bond and C—N bond, respectively, while on pathway (3), the A molecule goes back to the Franck-Condon structure on the ground electronic state. $S_{1,TS}$ is the excited transition state on the S_1 potential surface between the minimum structure $S_{1,min}$ and conical intersection $(S_1/S_0)_{CI(1)}$. $S_{0,IM(1)(2)}$ are the intermediate states on the ground electronic state surface S_0 following $(S_1/S_0)_{CI(1)(2)}$. $S_{0,TS3(a)(b)}$ are the transition states on the S_0 potential surface between Franck-Condon structure $S_{0,FC}$ and the intermediate states $S_{0,IM(1)(2)}$. $S_{0,NO(1a)(1b)(2)}$ are molecules with NO dissociated products on the S_0 state in different reaction channels.
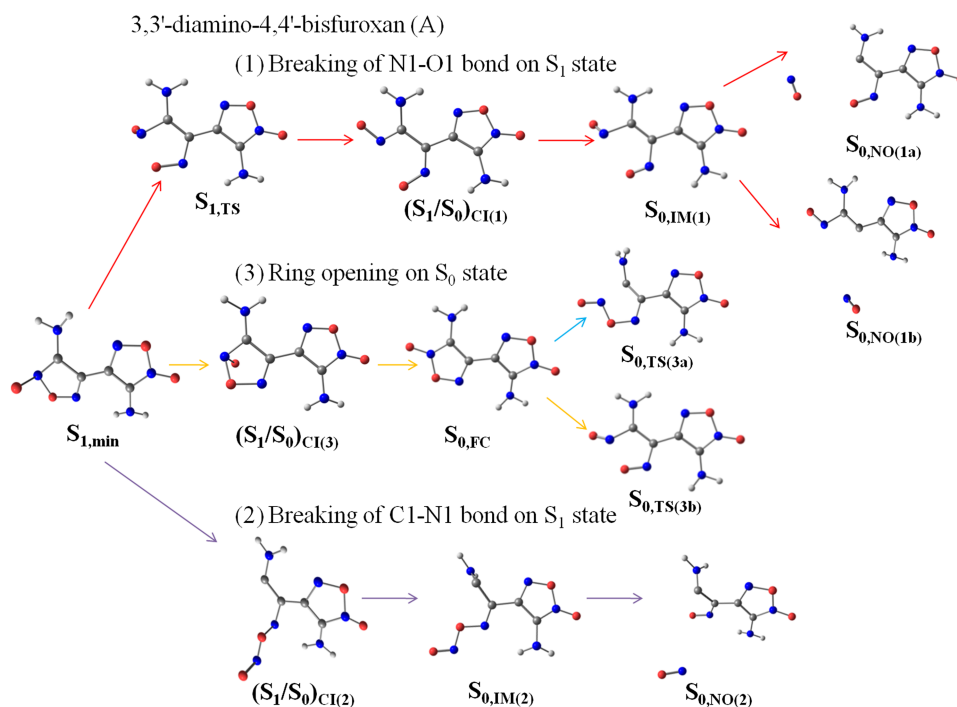

FIG. 7. Structures of all critical points and conical intersections mentioned in Figure 6 along three main dissociation reaction paths (1)–(3) for 3,3′-diamino-4,4′-bisfuroxan (A). For atoms in the structure, grey is carbon, blue is nitrogen, red is oxygen, and white is hydrogen.

state on the S_1 potential surface between the minimum structure $S_{1,min}$ and conical intersection $(S_1/S_0)_{CI(1)}$. $S_{0,IM(1)(2)}$ are the intermediate states on the ground electronic state surface S_0 following $(S_1/S_0)_{CI(1)(2)}$. $S_{0,TS3(a)(b)}$ are the transition states on the S_0 potential surface between Franck-Condon structure $S_{0,FC}$ and the intermediate states $S_{0,IM(1)(2)}$. $S_{0,NO(1a)(1b)(2)}$ are molecules with NO dissociated products on the S_0 state in different reaction channels. In Figure 6, the potential energies of each critical point are labeled: values in black are potential energies calculated via CASMP2(12,12)/6-31G(d), green numbers are calculated via CASSCF(12,12)/6-31G(d) without an MP2 correction, and red numbers are calculated via B3LYP/6-31G(d) and TD-DFT/6-31G(d). In the discussion below, if it is not mentioned specifically, the potential energies employed for analysis and discussion are derived from the CASMP2(12,12)/6-31G(d) algorithm.

As shown in Figure 6, with single photon absorption, molecule A can be excited to an S_n (n > 2) excited state: it then evolves to the first excited singlet electronic state S_1 through several conical intersections among different excited electronic states. As conical intersections between highly excited electronic states (S_n, n > 2) are typically not accurately calculated through a CASSCF algorithm, accurate energies for these conical intersections are not listed; however, the concept that molecules move from higher electronic to lower electronic states through conical intersections is well-documented in many studies.

On the S_1 electronic excited state surface, the molecule undergoes a rapid internal conversion to the energy minimum structure $S_{1,min}$. Following this, the molecule encounters the energy barrier for the transition state $S_{1,TS}$, and moves to the ground electronic state through conical intersections $(S_1/S_0)_{CI(1)-(3)}$ (transition states are not found between $S_{1,min}$ and $(S_1/S_0)_{CI(2)(3)}$): molecules undergoing this process would place sufficient vibrational energy in the S_0 state, transferred from the S_1 (and S_n) electronic energy, to dissociate. Totally three different conical intersections between S_0 and S_1 surface are identified related to reaction paths (1)–(3).

Reaction path (1), the red one in Figure 6, has the lowest transition state energy. Along this reaction coordinate (red path), molecule A moves from $S_{1,min}$, surmounts a 0.11 eV energy barrier at $S_{1,TS}$, and then reaches conical intersection $(S_1/S_0)_{CI(1)}$. Because the red path has the lowest energy barrier, this channel might be the most probable reaction path for the fragmentation: the furoxan ring opens at the N1—O1 bond (atoms labeled in Figure 1) along this coordinate.

Along reaction path (2), the furoxan ring opens via the C1—N1 bond. From $S_{1,min}$, molecule A surmounts an energy barrier of 1.34 eV and forms conical intersection $(S_1/S_0)_{CI(2)}$, shown in purple in Figure 6. This is not the minimum energy decomposition path for molecule A, but path (2) is energy available for the single photon absorption experimental system. Thus, reaction path (2) is also considered as one of the reasonable decomposition path for molecule A.
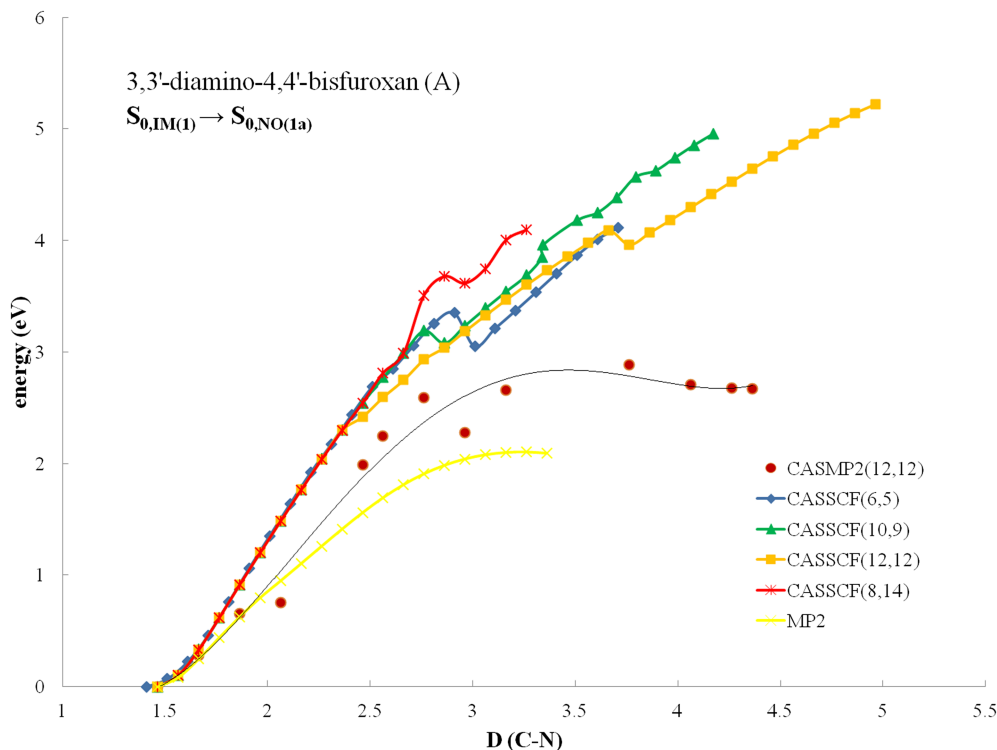

FIG. 8. Plots of NO dissociation along reaction path (1) for 3,3′-diamino-4,4′-bisfuroxan (A) from intermediate $S_{0,IM(1)}$ to $S_{0,NO(1a)}$ at different theoretical levels: (♦) CASSCF(6,5)/6-31G(d), (▲) CASSCF(10,9)/6-31G(d), (■) CASSCF(12,12)/6-31G(d), (*) CASSCF(8,14)/6-31G(d), (×) MP2/6-31G(d), (●) CASMP2(12,12)/6-31G(d). The x-axis is the distances between atom C1 and atom N1 (labels in Figure 1) and the y-axis is the potential energy surface along this coordinate for the ground electronic state. Based on pure, uncorrected CASSCF methods, as the NO group moves further from the rest of the molecule (>4.5 Å), the potential energy of the system increases (>5 eV); actual dissociation of NO under this algorithm is not apparent. After the CASMP2 energy correction, the potential energy for NO product release stabilizes at ~2.53 eV as the NO separation distance from the remaining bisfuroxan parent species increases beyond 3.5 Å: this latter range is close to that calculated by the direct MP2 method.

To form an NO product, the furoxan ring can also open via the C2—N2 bond, as well; however, no conical intersection related to the breaking of C2—N2 bond is found between S_1 and S_0 electronic states in this system. This suggests that the C2—N2 bond rupture reaction channel incorporates a slow, statistical, intramolecular vibrational redistribution, Fermi's Golden Rule, mechanism for NO generation, and will therefore be at best a secondary pathway for NO generation.

If the furoxan ring does not open on the first excited state S_1, molecule A can move from the $S_{1,min}$ to $S_{0,FC}$ on the ground electronic state through conical intersection $(S_1/S_0)_{CI(3)}$ (reaction path (3) in orange in Figure 6). As shown in Figure 7, the structure of $(S_1/S_0)_{CI(3)}$ is similar to that of $S_{1,min}$ with an energy barrier of 0.33 eV, 0.22 eV higher than that for the breaking of the N1—O1 bond on the S_1 state. Therefore, a strong competition or interference between reaction paths (1) and (3) must be present for the fragmentation of the electronically excited parent (A).

The adiabatic energy gaps between the S_1 and S_0 surfaces near conical intersections $(S_1/S_0)_{CI(1)-(3)}$ are computed to be in the range between 22 and 77 cm^{-1}; the S_1 and S_0 surfaces are thus strongly non-adiabatically coupled with one another. The small adiabatic energy gap increases the strength of the non-adiabatic coupling of the surfaces and the probability of a non-adiabatic transition from the upper to lower electronic states. As the molecule evolves from the S_1 to S_0 state through $(S_1/S_0)_{CI(1)-(3)}$, the IRC algorithm shows that

the steepest descent pathway for the molecule is to evolve to stable intermediate states $S_{0,im(1)(2)}$ along reaction paths (1) and (2) or to the stable Franck-Condon structure $S_{0,FC}$ along reaction path (3). From the IRC scan through reaction paths (1) and (2), the furoxan ring remains open at the intermediate states $S_{0,IM(1)(2)}$ following $(S_1/S_0)_{CI(1)(2)}$. The molecule then surmounts energy barriers in the range between 2.48 and 2.83 eV and forms NO products $S_{0,NO(1a)(1b)(2)}$. Structures of the three dissociated molecules with NO products can be found in Figure 7. From intermediate $S_{0,IM(1)}$, NO dissociates through rupture of either the C1—N1 or C2—N2 bond (labeled (a) and (b), respectively, in Figures 6 and 7) and from intermediate $S_{0,IM(2)}$, NO dissociates through the rupture of N1—O1 bond. For the decomposition of NO from $S_{0,im(1)(2)}$, different calculation levels (including CASSCF(6,5), CASSCF(10,9), CASSCF(12,12), CASSCF(8,14), CASMP2(12,12), B3LYP, and MP2) are applied in order to find the correct dissociation energy: results of these calculations are shown in Figures 8–10. Based on pure CASSCF methods, as the NO group moves further from the rest of the molecule (>4.0 Å), the potential energy of the system increases (>5 eV); actual dissociation of NO under this algorithm is not apparent. Moreover, the number of orbitals and electrons chosen for the included CASSCF methods does not affect this theoretical dissociation result. This obvious problem can be ameliorated by inclusion of higher electronic states for the multi-reference state, configuration interaction (CI) description that is apparently required
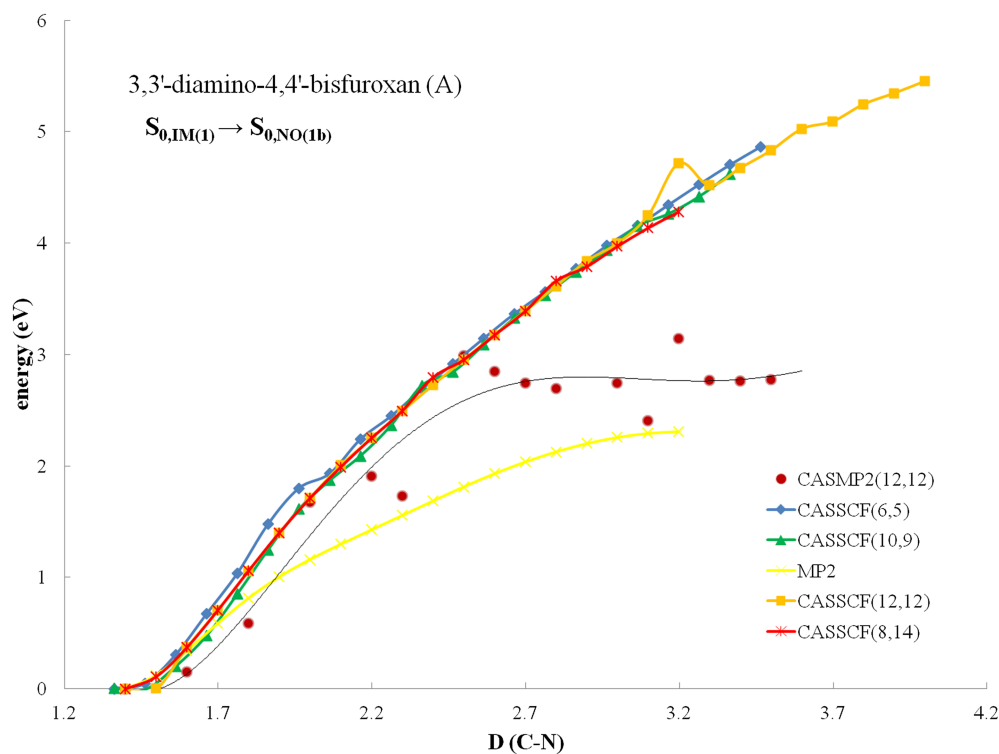

FIG. 9. Plots of NO dissociation in reaction path (1) of 3,3′-diamino-4,4′-bisfuroxan (A) from intermediate $S_{0,IM(1)}$ to $S_{0,NO(1b)}$ at different theoretical levels: (♦) CASSCF(6,5)/6-31G(d), (▲) CASSCF(10,9)/6-31G(d), (■) CASSCF(12,12)/6-31G(d), (*) CASSCF(8,14)/6-31G(d), (×) MP2/6-31G(d), (●) CASMP2(12,12)/6-31G(d). The x-axis is the distances between atom C2 and atom N2 (labels in Figure 1) and the y-axis is the potential energy surface along this coordinate on the ground electronic state. Based on pure CASSCF methods, as the NO group moves further from the rest of the molecule (>3.7 Å), the potential energy of the system increases (>5 eV); actual dissociation of NO under this algorithm is not apparent. After the CASMP2 energy correction, the potential energy for NO product release becomes stable at 2.61 eV as the NO separation distance from the remaining bisfuroxan parent increases beyond 3.0 Å: this latter range is close to that calculated by direct MP2 method.
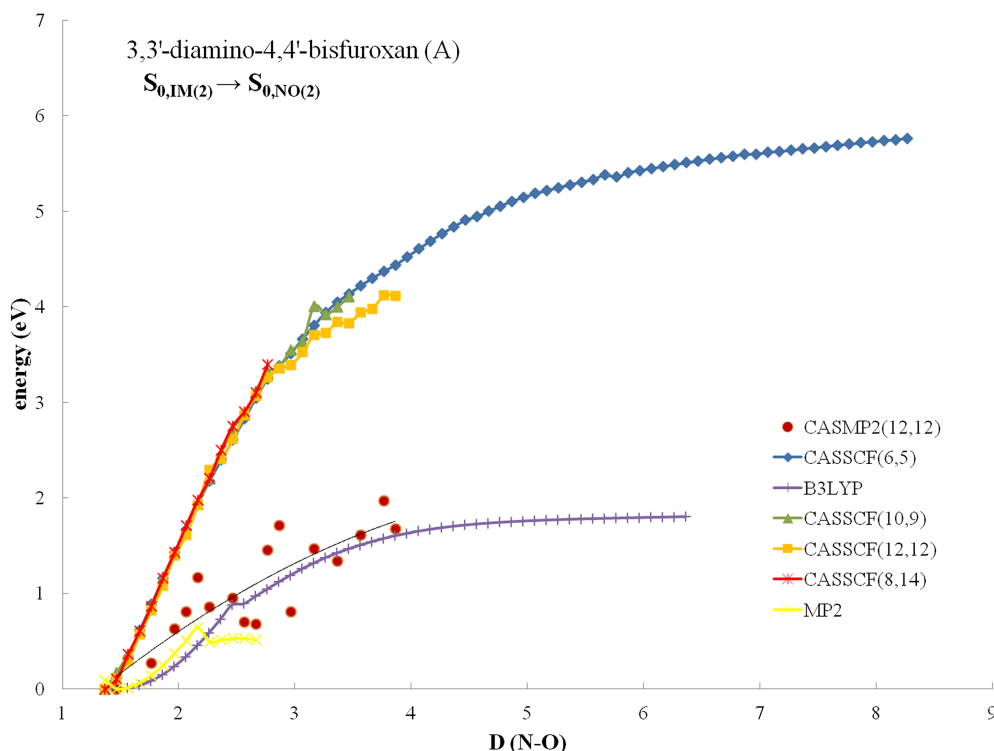
FIG. 10. Plots of NO dissociation in reaction path (2) of 3,3′-diamino-4,4′-bisfuroxan (A) from intermediate $S_{0,IM(2)}$ to $S_{0,NO(2)}$ in different theoretical levels: (♦) CASSCF(6,5)/6-31G(d), (▲) CASSCF(10,9)/6-31G(d), (■) CASSCF(12,12)/6-31G(d), (*) CASSCF(8,14)/6-31G(d), (+) B3LYP/6-31G(d), (●) CASMP2(12,12)/6-31G(d). The x-axis is the distances between atom N1 and atom O1 (labels in Figure 1) and the y-axis is the potential energy surface on the ground electronic state. Based on pure CASSCF methods, as the NO group moves further from the rest of the molecule (>4.5 Å), the potential energy of the system increases (>5 eV); actual dissociation of NO under this algorithm is not apparent. Subsequent to the CASMP2 energy correction, the potential energy for NO product release becomes stable at 3.13 eV as the NO separation distance from the remaining bisfuroxan parent is greater than 3.5 Å: this latter range is close to that calculated by direct B3LYP method.

for the unique potential energy surfaces and chemistry of these molecules: this strong state mixing is clearly a function of the system structure. In fact, the potential energy for NO dissociation becomes stable (1.5–2.0 eV) when the NO product is about 3.0–3.5 Å away from the rest of the molecule, employing DFT (B3LYP) and MP2 calculational methods.

The B3LYP method is not presented in the NO dissociation from the $S_{0,IM(1)}$ intermediate state (Figures 8 and 9) on reaction path (1) because the stable structure $S_{0,IM(1)}$ is only identified by the CASSCF and MP2 methods. This is addressed in more detail from the ground state decomposition potential energy surface in the next few paragraphs. Employing optimized geometries based on a CASSCF(12,12) and correcting the energies at the CASMP2 level for each point in the bond length scan, an energy corrected CASMP2(12,12) scan is obtained. The potential energy for NO product release becomes stable in the range between 2.48 and 2.83 eV under a CASMP2 calculation, as the NO separation distance from the remaining bisfuroxan parent reaches 3.0–3.5 Å: this latter range is close to that calculated by either direct MP2 or B3LYP methods.

The dissociation energy of NO based on CASSCF methods without an MP2 correction is higher than the laser energy limit in our experiment, implying that, based on the result of a pure CASSCF calculation without an MP2 correction along the IRC minimum energy pathway as a function of the separation distance, an NO product should not be observed. Since NO is

detected in the experiment, the results of the CASMP2 method (DFT, as well) are more reliable than those of the pure CASSCF calculations, even at the (12,12) level and independent of the basis set size. We can conclude, therefore, that an MP2 correction to the CASSCF algorithm is essential for calculation of the reaction surface for this fragmentation. Multi-reference state CI is apparently a strong function of the structure (based on CASSCF calculations) of the evolving NO dissociation from its bisfuroxan parent. A detailed comparison of molecular orbitals of the final molecular structure $S_{0,NO(2)}$ with NO product for different theoretical levels CASMP2(12,12)/6-31G(d), B3LYP/6-31G(d), and CASSCF(12,12)/6-31G(d) is shown in Figure S1 of the supplementary material.

Molecule A moves along reaction pathway (3) back to the Franck-Condon structure $S_{0,FC}$. To create an NO product by this mechanism, the furoxan ring can open from $S_{0,FC}$ on the ground electronic state with energy barriers either 1.24 eV (breaking of the O1—N1 bond) or 1.96 eV (breaking of the C1—N1 bond). This result is consistent with previous studies for ground state dissociation of A that suggest the most favorable (thermal) decomposition process for furoxan is ring opening via the endocyclic N—O bond closer to the N-oxide group with an energy barrier of 0.98 eV (94.62 KJ/mol).[2] The two energy barriers are energy available in the present experimental system and, similar to the furoxan ring on the S_1 state, the N1—O1 bond is more active than the C—N bond. Figure 11 shows the opening of the furoxan ring on the S_0
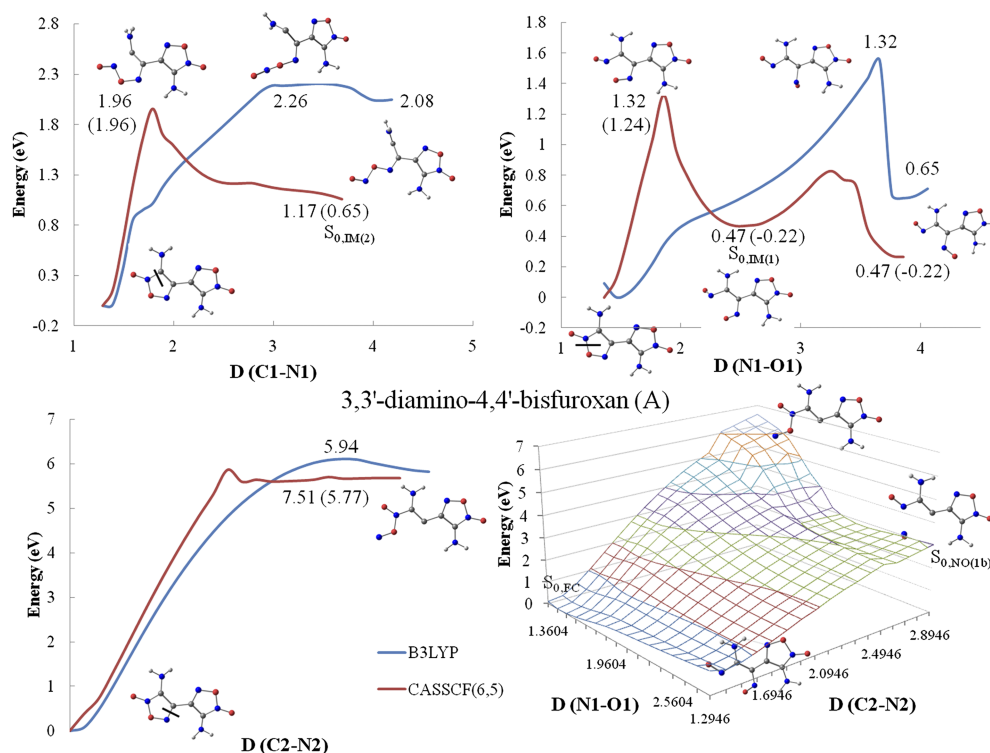
FIG. 11. Plot of the opening of the furoxan ring on the S_0 state through the breaking of bonds C1—N1 (top left), N1—O1 (top right), and C2—N2 (bottom left) calculated with methods CASSCF(6,5) (red) and B3LYP (blue) employing basis set 6-31G(d). Values on the potential surfaces are energies of critical points (transition and stable intermediate states). Energy values in parentheses are potential energies based on CASMP2(12,12) algorithm. The diagram on the bottom right is a 3-D energy vs. distance plot for the N1—O1 and C2—N2 separations employing the B3LYP method: the x-axis is the distance between atoms N1 and O1, the y-axis is the distance between atoms C2 and N2, and the z-axis is the potential energy surface for the ground electronic state surface. The N1—O1 distance is the most active bond of the furoxan ring on the ground state surface: if the ring opens on the S_0 state, both C2—N2 and O1—N1 bonds most likely break simultaneously. $S_{0,FC}$, $S_{0,IM(1)}$, $S_{0,IM(2)}$, and $S_{0,NO(b)}$ referred to in this figure are the same Frank-Condon structure, intermediate state, and NO dissociation structures depicted in Figures 6 and 7.

state through the breaking of bonds C1—N1 (top left), N1—O1 (top right), and C2—N2 (bottom left) calculated with methods CASSCF(6,5) (red) and B3LYP (blue) employing basis set 6-31G(d). Values on the potential surfaces are energies of critical points (transition and stable intermediate states), and values in parentheses are potential energies based on CASMP2(12,12). The $S_{0,FC}$ structure of A employing CASSCF and B3LYP methods is not exactly the same as discussed in Section V A: their ground state potential surfaces for the furoxan ring opening are different as well (see Figure 11). The top right diagram of this figure shows the potential energy vs. the dissociation bond length for the N1—O1 bond. At the B3LYP scan, the potential energy of the system increases with bond length as the furoxan ring opens and atom O1 moves further from atom N1. A steep drop in the potential energy occurs (B3LYP) when the distance between N1 and O1 atoms is greater than 3.5 Å. A CASSCF(6,5) scan, however, finds an intermediate state along the calculated surface when the distance of N1 and O1 atoms is around 2.5 Å; the potential energy of this intermediate is −0.22 eV following a CASMP2 calculation. This stable intermediate structure is not found at the B3LYP level scan. This latter intermediate is the $S_{0,IM(1)}$ structure in Figures 6 and 7 and the beginning structure for the NO dissociations depicted in Figures 8 and 9. Since no related point for this intermediate is located by the B3LYP method, this algorithm is not represented in Figures 8 and 9 for the NO dissociation scan. Although conical intersections

related to the breaking of C2—N2 bond are not found theoretically, the breaking of C2—N2 bond is another way to open the furoxan ring on the S_0 state in order to separate an NO product, as shown in the bottom two diagrams of Figure 11. If the C2—N2 bond breaks first, the energy barrier is higher than 5 eV (diagram in bottom left of Figure 11); however, if the C2—N2 bond and O1—N1 bond break at the same time, as shown in the 3-D diagram in bottom right of Figure 11, the energy barrier is much lower. Along this compound pathway the NO product is completely dissociated from the system with an energy barrier of 2.83 eV. The product state has same structure ($S_{0,NO(1b)}$) as shown for reaction path (1b) in Figures 6 and 7. Therefore, the furoxan ring of molecule A can open either on the first excited electronic state S_1 surface or on the ground electronic state S_0 surface. If the ring opens on the S_0 state, both C2—N2 and O1—N1 bonds most likely break simultaneously.

Energies of the final molecular structures with a dissociated NO product along reaction paths (1)–(3) are in the range 2.53–3.13 eV; thus, dissociation products should thereby have warm vibrational temperatures as the energy in the molecule from electronic excitation is now transferred and stored as vibrational energy on the ground electronic state surface. These final dissociation energies for A are about 1–2 eV higher compared to other energetic materials investigated previously by similar means.[38–40] Based on the present experimental results, the vibration temperature of NO is 1170 K, about

1000 K lower than that found for other comparable energetic materials (for example, dinitro-pyrazole (DNP), FOX-7, and TKX-50).[38–40] The NO product moves away from the rest of the molecule or radical without obvious torque for all the reaction channels as shown in Figure 7. Therefore, NO products should have low rotational temperatures, as is consistent with experimental results.

In sum, molecule A absorbs one laser photon and is excited from the ground state to higher electronic states. The electronic excitation models the condensed phase, triboluminescent processes that occur upon a shock wave, etc., and crystal initiation of the energy release processes. Molecule A then decomposes to form NO product, potentially following three possible reaction paths, as outlined in Figure 6. The furoxan ring of A opens either on the first excited state S_1 surface or on the ground electronic state S_0 surface. If the furoxan ring opens on the S_1 state, the breaking of N1—O1 bond has a much lower energy barrier than does the breaking of the C1—N1 bond, following which NO dissociation occurs on the ground electronic state S_0. If the furoxan ring opens on the ground state S_0, the N1—O1 and C2—N2 bonds most likely break together, implying that the opening of a furoxan ring and the dissociation of NO product occur simultaneously. In the final NO dissociation scan, CASSCF methods cannot provide reasonable potential energy surfaces through variation of orbital and electron number, and basis set. Applying an MP2 correction to the CASSCF algorithm, the CASMP2 calculation yields a similar dissociation potential surface to those generated by MP2 and B3LYP methods. The decomposition dynamics are purely non-adiabatic in nature and conical intersections lead rapidly and efficiently to internal conversion from upper to lower electronic states through non-adiabatic, radiationless transitions. During this internal conversion, electronic energy in the upper state is converted to vibrational energy on the lower states on a potential time scale of a few tens of femtoseconds. Based on these calculations, NO should have a warm vibrational temperature, as is consistent with experimental results. The final molecular structures with NO product are about 2.5–3.0 eV higher in energy than that of the Franck-Condon structure $S_{0,FC}$.

The relatively lower vibrational temperature of the NO product compared to that for other energetic materials investigated makes diamino-bisfuroxan molecule A different.[38–40] With a high vibrational temperature, the residual parent molecule related energetic species can continue to execute secondary decomposition reactions in both isolated and high density, condensed phase energetic systems. With a warm NO vibrational temperature, it too can further engage in subsequent condensed phase reactivity. The low rotational temperature of the fragmented NO indicates that the final bond rupture for the initial fragmentation reaction generates little torque on the NO molecule as it leaves the parent molecule. The theoretical and experimental results are in agreement here as well. This is yet another demonstration that the calculations and experiments support one another, and therefore that the theoretical approach to these kinetics, dynamics, and mechanisms can be of predictive value for properties and behaviors of these large organic energetic molecules not presently readily measured by experiments.

C. Potential energy surfaces for 4,4′-diamino-3, 3′- bisfuroxan B

Decomposition mechanisms for molecule B are similar to those of molecule A. In the paragraphs below, a brief description of the decomposition mechanisms for molecule B, especially as they differ from those for molecule A, will be presented.

Schematic one-dimensional projections of the multidimensional singlet potential energy surfaces (S_0 and S_1) of 4,4′-diamino-3,3′-bisfuroxan (B), with locations and potential energies (the presented energies are not corrected for zero point energy) for different critical points and conical intersections along several energy available reaction paths, are plotted in Figures 12 and 13. The reaction coordinates depicted in Figure 12 include C—N and N—O bond lengths within the furoxan rings: with red, orange, purple, and blue arrows in Figure 12 indicate different possible decomposition channels or reaction pathways for B following excitation to its first excited singlet state S_1. The structures of critical points and conical intersection are summarized in Figure 13. The potential energy of each critical point is labeled in Figure 12. In the discussion below, if it is not mentioned specifically, the potential energies discussed are from CASMP2(12,12)/6-31G(d) calculations.

As shown in Figure 12, molecule B undergoes a rapid (~10 fs) internal conversion to the energy minimum structure $S_{1,min}$. Following this, B encounters the energy barrier for transition state $S_{1,TS}$, and moves to the ground electronic state through conical intersections $(S_1/S_0)_{CI(1)–(3)}$ (no transition state is located between $S_{1,min}$ and $(S_1/S_0)_{CI(2)(3)}$): totally three different conical intersections between the S_0 and S_1 surfaces are identified related to reaction paths (1)–(3).

Reaction path (1) (the red one in Figure 12) has the lowest transition state (barrier) energy (0.11 eV), and this channel might be the most probable reaction path for the fragmentation: the furoxan ring opens at the N1—O1 bond (atoms labeled in Figure 1) along this reaction coordinate. The furoxan ring opens via the C1—N1 bond along reaction path (2). From $S_{1,min}$, molecule B surmounts an energy barrier of 1.83 eV and forms the conical intersection $(S_1/S_0)_{CI(2)}$ (purple in Figure 12). If the furoxan ring does not open on the first excited state S_1, molecule B can move from $S_{1,min}$ to $S_{0,FC}$ on the ground electronic state through conical intersection $(S_1/S_0)_{CI(3)}$, which is reaction path (3) (orange in Figure 12) with an energy barrier of 0.50 eV.

The adiabatic energy gaps between S_1 and S_0 surfaces near conical intersections $(S_1/S_0)_{CI(1)–(3)}$ are computed to be in the range between 7 and 44 cm^{-1}. As the molecule moves from S_1 to S_0 state through $(S_1/S_0)_{CI(1)–(3)}$, the IRC algorithm shows that the steepest descent pathway for the molecule is to evolve to stable intermediate states $S_{0,im(1)(2)}$ along reaction paths (1) and (2) or to the stable Franck-Condon structure $S_{0,FC}$ along reaction path (3). Following reaction path (1) from $S_{0,IM(1)}$, the molecule then surmounts energy barriers in the range between 2.43 and 3.34 eV and forms NO products $S_{0,NO(1a)(1b)}$. In this case, NO dissociates through either the C2—N2 or C1—N1 ring bonds (labeled (a) and (b) in Figures 12 and 13). Along reaction path (2), intermediate
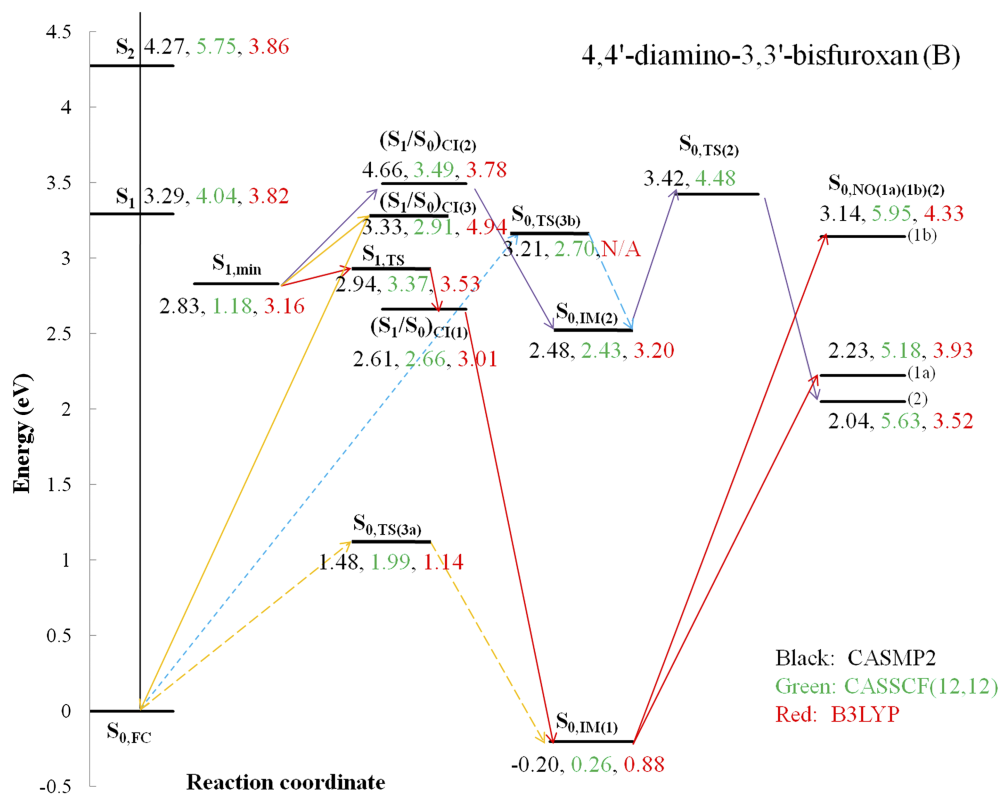
FIG. 12. A schematic one-dimensional projection of the multi-dimensional energy surfaces for 4,4′-diamino-3,3′-bisfuroxan (B) dissociation paths computed at the CASSCF(12,12)/6-31G(d), CASMP2(12,12)/6-31G(d), and TD-DFT(DFT)/6-31G(d) levels of theory. The diagram is plotted based on the potential energies from the CASMP2 algorithm. The potential energy of each critical point on this path, as calculated by each algorithm, is labeled: values in black are potential energies calculated via CASMP2(12,12)/6-31G(d), green numbers are calculated via CASSCF(12,12)/6-31G(d) without MP2 correction, and red numbers are calculated via B3LYP/6-31G(d), and TD-DFT/6-31G(d). The red, orange, purple, and blue arrows represent different reaction channels for NO dissociation. FC geometry $S_{0,FC}$ is the optimized minimum energy of B in the S_0 state, and $(S_1/S_0)_{CI(1)-(3)}$ are conical intersections between the S_0 and S_1 states. Along pathways (1) and (2), the furoxan ring opens through the N—O bond and C—N bond, respectively, while on pathway (3), the B molecule goes back to the Franck-Condon structure on the ground electronic state. $S_{1,TS}$ is the excited transition state on the S_1 potential surface between the minimum structure $S_{1,min}$ and conical intersection $(S_1/S_0)_{CI(1)}$. $S_{0,IM(1)(2)}$ are the intermediate states on the ground electronic state surface S_0 following $(S_1/S_0)_{CI(1)(2)}$. $S_{0,TS3(a)(b)}$ are the transition states on the S_0 potential surface between Franck-Condon structure $S_{0,FC}$ and the intermediate states $S_{0,IM(1)(2)}$. $S_{0,NO(1a)(1b)(2)}$ are molecules with NO dissociated products on the S_0 state in different reaction channels.

state $S_{0,IM(2)}$ surmounts an energy barrier of 0.94 eV through transition state $S_{0,TS(2)}$ and forms the NO product $S_{0,NO(2)}$ at potential energy 2.04 eV. A transition state exists along this
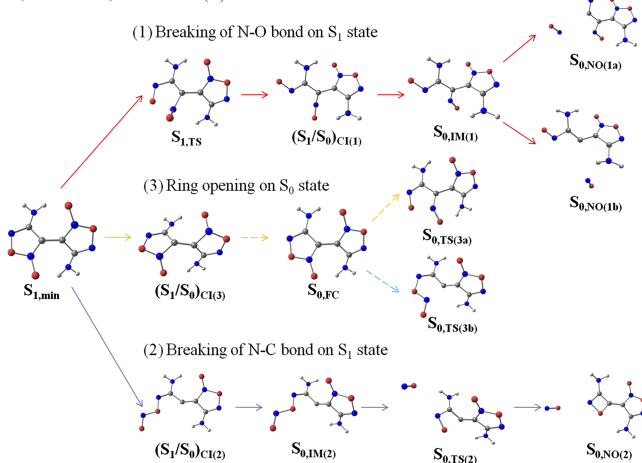

FIG. 13. Structures of all critical points and conical intersections referred in Figure 12 along three main dissociation reaction paths (1)–(3) of 4,4′-diamino-3,3′-bisfuroxan (B). For atoms in the structure, grey is carbon, blue is nitrogen, red is oxygen, and white is hydrogen.

fragmentation channel because a stable rectangular structure is formed at $S_{0,NO(2)}$: this exit structure lowers the molecular energy of the system as shown in Figure 14.

For the decomposition of NO from $S_{0,im(1)(2)}$, different calculation levels (including CASSCF(6,5), CASSCF(10,9), CASSCF(12,12), CASSCF(8,14), CASMP2(12,12), B3LYP, and MP2) are applied in order to find the correct dissociation energy. The results of these calculations are presented in Figures 14–16; dissociation of NO apparently does not occur for the system along reaction pathways (1) and (2) according to all pure CASSCF calculations. The CASMP2(12,12) algorithm yields a potential energy for the NO product, which stabilizes in the range between 2.23 and 3.14 eV when the NO fragment is 3.0–3.5 Å from the rest of the molecule: this result is close to that determined by either the MP2 or B3LYP IRC scan methods. A detailed comparison of molecular orbitals of the final molecular structure $S_{0,NO(1a)}$ with NO product for the different theoretical levels CASMP2(12,12)/6-31G(d), B3LYP/6-31G(d), and CASSCF(12,12)/6-31G(d) is shown in Figure S2 of the supplementary material. In reaction path (2), the transition state and formation of a rectangular structure (Figure 16) are well determined by all the theoretical methods except B3LYP. The MP2 method shows an NO dissociated
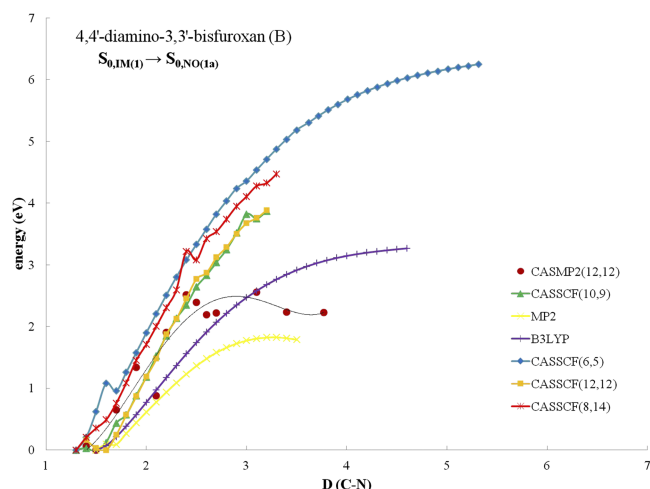
FIG. 14. Plots of NO dissociation along reaction path (1) for 4,4′-diamino-3,3′-bisfuroxan (B) from intermediate $S_{0,IM(1)}$ to $S_{0,NO(1b)}$ in different theoretical levels: (♦) CASSCF(6,5)/6-31G(d), (▲) CASSCF(10,9)/6-31G(d), (■) CASSCF(12,12)/6-31G(d), (*) CASSCF(8,14)/6-31G(d), (×) MP2/6-31G(d), (+) B3LYP/6-31G(d), (●) CASMP2(12,12)/6-31G(d). The x-axis is the distance between atoms C2 and N2 (labels in Figure 1) and the y-axis is the potential energy path value on the ground electronic state. Based on pure CASSCF methods, as the NO group moves further from the rest of the molecule (>3.5 Å), the potential energy of the system increases (>5 eV); actual dissociation of NO under this algorithm is not apparent. Potential energy for NO product release becomes stable in 2.23 eV as the NO separation distance from the remaining bisfuroxan parent is greater than 3.0 Å: this latter distance is close to that calculated by direct MP2 and B3LYP methods.

structure at the end of the IRC scan with a much lower potential energy because the structure of the furoxan ring at the MP2 level has changed greatly, as shown in Figure 16. The
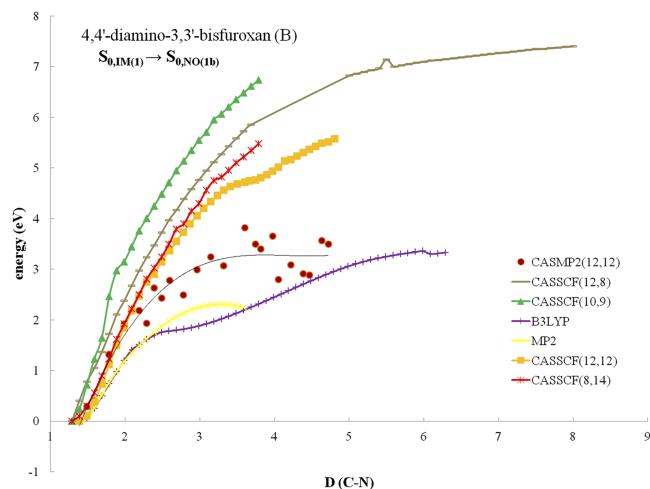
dissociation energy of NO in the various CASSCF methods without an MP2 correction is close to or even higher than the laser limit in our experiment; this implies that, based on the results of a pure CASSCF approach, no NO product should be observed for the decomposition. Since NO is detected following S_1 excitation, the results of the CASMP2 method are more reasonable from both a theoretical and experimental point of view.

Molecule B moves along reaction path (3) back to the Franck-Condon structure $S_{0,FC}$. To create an NO product for this fragmentation channel, the furoxan ring can open from $S_{0,FC}$ on the ground electronic state surface by surmounting an energy barrier of either 1.48 eV (breaking the N1—O1 bond) or 3.21 eV (breaking the C1—N1 bond). These two potential energy pathways are energy available under the experimental conditions. Figure 17 shows the opening of furoxan ring on the S_0 state surface through the breaking of bonds C1—N1 (top left), N1—O1 (top right), and C2—N2 (bottom left) calculated through methods CASSCF(6,5) (red) and B3LYP (blue) with basis set 6-31G(d). If the C2—N2 bond breaks first, the energy barrier is higher than 5 eV (bottom left of Figure 17); however, if the C2—N2 and N1—O1 bonds break simultaneously, as shown in the 3-D diagram at the bottom right of Figure 17, the energy barrier is much lower: NO product creation along pathway (3) for this two bond reaction coordinate has a combined energy barrier of 2.23 eV with the same dissociation structure $S_{0,NO(1a)}$ shown for reaction path (1a) (Figures 12 and 13).

Energies of the final molecular structures with a dissociated NO product generated through reaction paths (1)–(3)
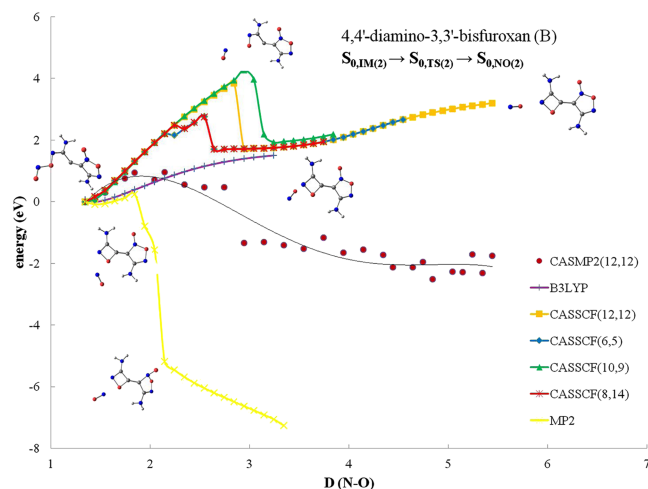

FIG. 15. Plots of NO dissociation in reaction path (1) for 4,4′-diamino-3,3′-bisfuroxan (B) from intermediate $S_{0,IM(1)}$ to $S_{0,NO(1a)}$ at different theoretical levels: (♦) CASSCF(6,5)/6-31G(d), (▲) CASSCF(10,9)/6-31G(d), (■) CASSCF(12,12)/6-31G(d), (*) CASSCF(8,14)/6-31G(d), (×) MP2/6-31G(d), (+) B3LYP/6-31G(d), (●) CASMP2(12,12)/6-31G(d). The x-axis is the distance between atom C1 and atom N1 (labels in Figure 1) and the y-axis is the potential energy path value on the ground electronic state. Based on pure CASSCF methods, as the NO group moves further from the rest of the molecule (>3.0 Å), the potential energy of the system increases (>5 eV); actual dissociation of NO under this algorithm is not apparent. Potential energy for NO product release becomes stable around 3.14 eV under a CASMP2 energy calculation as the NO separation distance from the remaining bisfuroxan parent is greater than 3.5 Å: this latter distance is close to that calculated by direct MP2 and B3LYP methods.

FIG. 16. Plots of NO dissociation along reaction path (2) for 4,4′-diamino-3,3′-bisfuroxan (B) from intermediate $S_{0,IM(2)}$ to $S_{0,NO(2)}$ at different theoretical levels: (♦) CASSCF(6,5)/6-31G(d), (▲) CASSCF(10,9)/6-31G(d), (■) CASSCF(12,12)/6-31G(d), (*) CASSCF(8,14)/6-31G(d), (×) MP2/6-31G(d), (+) B3LYP/6-31G(d), (●) CASMP2(12,12)/6-31G(d). The x-axis is the distance between atom N1 and atom O1 (labels in Figure 1) and the y-axis is the potential energy path value on the ground electronic state. The transition state and formation of a rectangular structure are well determined by all the theoretical methods except B3LYP. The MP2 method renders an NO dissociation structure at the end of the IRC scan with a much lower potential energy because the structure of the furoxan ring at the MP2 level has changed greatly. After the CASMP2 energy correction, the potential energy for NO product release becomes stable at ~2.04 eV as the NO separation distance from the remaining bisfuroxan parent increases beyond 4.0 Å.
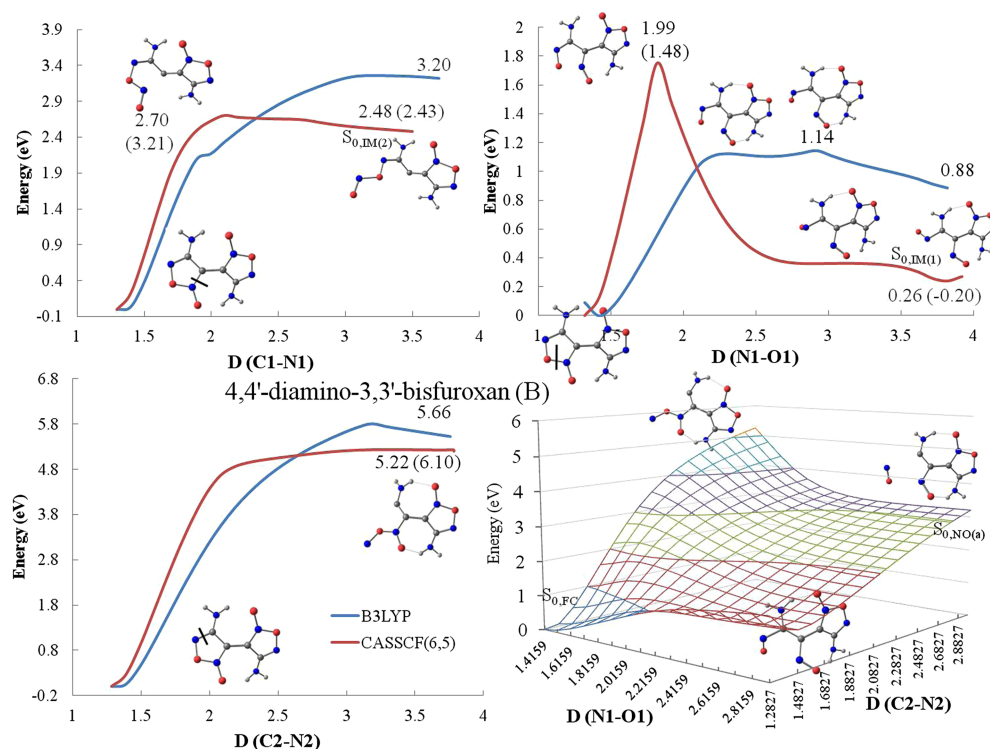
FIG. 17. Plot of the opening of the furoxan ring on the S_0 state through the breaking of bonds C1—N1 (top left), N1—O1 (top right), and C2—N2 (bottom left) calculated with methods CASSCF(6,5) (red) and B3LYP (blue) employing basis set 6-31G(d). Values on the potential surfaces are energies of critical points (transition and stable intermediate states). Energy values in parentheses are potential energies based on CASMP2(12,12) algorithm. The diagram on the bottom right is a 3-D energy vs. distance plot for the N1—O1 and C2—N2 separations employing the B3LYP method: the x-axis is the distance between atoms N1 and O1, the y-axis is the distance between atoms C2 and N2, and the z-axis is the potential energy surface for the ground electronic state surface. The N1—O1 distance is the most active bond of the furoxan ring on the ground state surface: if the ring opens on the S_0 state, both C2—N2 and O1—N1 bonds most likely break simultaneously. $S_{0,FC}$, $S_{0,IM(1)}$, $S_{0,IM(2)}$, and $S_{0,NO(a)}$ referred to in this figure are the same Frank-Condon structure, intermediate state, and NO dissociation structures depicted in Figures 12 and 13.

(i.e., by mechanisms (1)–(3)) are in the range 2.04–3.14 eV: these, dissociation products should have warm vibrational temperatures (ca. 1000 K), as the energy in the molecule from photon absorption is now transferred and stored as vibrational energy on the ground electronic state surface. The NO product moves away from the rest of the molecule or residual radical without obvious torque for all the reaction channels as shown in Figure 13. Therefore, NO products should have low rotational temperatures, as it is consistent with experimental results.

In sum, molecule B has similar decomposition mechanisms to molecule A. Once excited from its ground state to higher electronic states, it decomposes to form an NO product, following three possible reaction paths, as outlined in Figure 12. The furoxan ring of B opens either on the first excited state S_1 or on the ground electronic state S_0. The N1—O1 bond is the most reactive bond of the furoxan ring for NO dissociation. If the furoxan ring opens on the ground state S_0, most likely the N1—O1 and C2—N2 bonds break together through a compound reaction coordinate. CASMP2 calculations provide the most reasonable potential surface in the final NO dissociation scan. This important finding for the reaction path kinetics and dynamics implies that CI mixing of highly excited configurations and multi-reference state descriptions of the S_1 and S_0 states are reaction coordinate dependent and that consideration of such effects is essential for generating a proper mechanistic understanding of the experimental observations. The subsequent NO product generated through

the three available pathways has a warm vibrational temperature and a cold rotational temperature, which is consistent with the experimental results.

The main difference between molecule A and B initial decomposition mechanisms is that during the NO dissociation, molecule B can form a stable rectangular structure, which lowers the potential energy of the fragmenting system. This difference between A and B is related to the different positions of the NH_2 groups on the furoxan rings. Thus, due to the prospective formation of a stable intermediate structure in a reaction channel for B decomposition, more energy from higher electronic states can be transferred to the vibrational energy of NO. This exit channel stabilization for formation of an NO product for molecule B might be an explanation for the observation that NO from B has a higher vibrational temperature (1400 K) than does NO from A (1170 K). Other potential energy differences between A and B in the decomposition paths are mainly caused by intramolecular hydrogen bonds within molecule B.[12] The vibrational temperature of the initial dissociation product is important in recognizing energetic molecules because initial decomposition products with high vibrational excitation are able to propagate a chain reaction better following the initial stimulus, leading to detonation. The $S_n \rightarrow \cdots \rightarrow S_o$ pathways through a series of conical intersections leave the molecule on a new part of the S_0 potential energy surface, not necessarily near the FC equilibrium point.[44,45]

Diamino-bisfuroxan molecules A and B have comparable explosive properties to those of RDX, but their NO products have relatively lower vibrational temperatures than the NO product from RDX. This energy difference for the vibrational excitation of NO generated by the two different classes of energetic materials suggests that the energy partition between the NO product and the remaining large organic species might play a significant role in the energy release and propagation processes for energetic behavior of these systems.

VI. CONCLUSIONS

The decomposition of the unimolecular energetic molecules, 3,3′-diamino-4,4′-bisfuroxan (A) and 4,4′-diamino-3,3′-bisfuroxan (B), following electronic excitation has been explored via nanosecond, energy resolved spectroscopy. These two energetic molecules create NO as an initial decomposition product at the nanosecond excitation energies (5.0–5.5 eV). The NO product is vibrationally warm (1170 ± 50 K for A, 1400 ± 50 K for B) and rotationally cold (<55 K) NO products.

Based on CASSCF calculations, guided by experimental observations, the NO products are released by the opening of the furoxan ring of both A and B: breaking of the N1—O1 bond on the ring has the lowest energetic barrier. The furoxan ring opens either on the S_1 excited state or S_0 ground state potential energy surface, and, through ring-opening conical intersections $(S_1/S_0)_{CI(1)(2)}$, forms intermediate states on the S_0 surface. Both molecules may also traverse a ring-closed conical intersection $(S_1/S_0)_{CI(3)}$ and move back to the Franck-Condon structure on the S_0 state; along this reaction fragmentation channel, the ring opens on the ground electronic state S_0. For the ground state ring-opening decomposition reaction, the N—O and C—N bonds break together in order to create NO on the lowest energy reaction channel. Conical intersections are the key point for the theoretical mechanisms, as they provide nonadiabatic radiationless internal conversion between upper and lower electronic states on the fs time scale and place the undissociated molecule on the ground state potential surface with all its vibronic excitation energy placed in the ground state vibrations available for bond breaking.

Different theoretical methods are applied, including B3LYP, MP2, CASSCF(6,5), CASSCF(10,9), CASSCF(8,14), CASSCF(12,12), and CASMP2(12,12), to explore the NO fragmentation reaction on the ground state surface through various intermediate states. The uncorrected CASSCF methods predict that NO dissociation has a high energetic barrier of ~5 eV, rendering NO dissociation impossible in disagreement with experimental observation. The number of electrons and orbitals chosen for the CASSCF methods, and the basis sets employed does not affect this theoretical conclusion; however, through utilization of a corrected CASSCF algorithm CASMP2(12,12), the energetic barrier drops to ~3 eV. Interestingly, this valve is close to the ones calculated by B3LYP and MP2 methods. Therefore, an MP2 correction to the CASSCF algorithm is important in order to obtain reasonable values of the molecular potential energy surfaces for these molecules. Contribution of higher electronic configurations to the multi configurational CI is essential for an accurate rendering of the unique chemistry of these molecules, especially as it changes

with reaction coordinate. Although the DFT B3LYP method is not completely consistent with the CASSCF/MP2 result, especially for ground state ring-opening scans, it is generally a fast and good method with which to estimate the surface/reaction coordinate behavior.

NO products are calculated to form on the ground state surface with little rotational excitation at the last NO dissociation step, which is consistent with the low rotational temperature of NO measured in the experiment. The experimental vibrational temperatures of NO products from both A and B are about 800–1000 K lower compared to previously studied energetic molecules with NO as an initial decomposition product. Theoretical results are consistent with these general observations, as the energy of the final NO product with the rest of the molecule is ~3 eV above the ground state Franck-Condon structure $S_{0,FC}$. Energy partitioning between the residual organic species and the fragmenting NO may additionally play a role in the vibrational excitation of NO and in the stored energy release from these energetic molecules. The vibrational temperature of the NO product of B is 230 K higher than that for A. Calculations provide an explanation for this observation: as NO dissociates from molecule B, the remaining organic species forms a stable rectangular intermediate structure in the exit channel, which lowers the overall potential energy of the complex by ~1 eV.

SUPPLEMENTARY MATERIAL

See supplementary material for molecular orbitals of the final decomposition structure $S_{0,NO(1a)}$ with NO product for the different theoretical levels CASMP2(12,12)/6-31G(d), B3LYP/6-31G(d), and CASSCF(12,12)/6-31G(d) of both energetic molecules 3,3′-diamino-4,4′-bisfuroxan (A) and 4,4′-diamino-3,3′-bisfuroxan (B) and a detailed comparison of molecular orbitals of the final molecular structure $S_{0,NO(2)}$ with NO product for different theoretical levels CASMP2(12,12)/6–31G(d), B3LYP/6-31G(d), and CASSCF(12,12)/6-31G(d).

ACKNOWLEDGMENTS

[1] Y. Li, Z. Zhang, Z. Ge, B. Wang, W. Lai, and Y. Luo, "Study of furoxan derivatives for energetic applications," Chin. J. Chem. **31**, 520 (2013).
[2] N. N. Makhova, I. V. Ovchinnikov, A. S. Kulikov, D. V. Khakimov, M. S. Molchanova, and T. S. Pivina, "Diaminofuroxan: Synthetic approaches and computer-aided study of thermodynamic stability," Propellants, Explos., Pyrotech. **37**, 549 (2012).
[3] V. Vsetecka, R. Fruttero, A. Gasco, and O. Exner, "Dipole moments and electron distribution of furoxans and furazans," J. Mol. Struct. **324**, 277 (1994).

[4]E. Sedano, C. Sarasola, J. M. Ugalde, and K. Fakultatea, "Conformations and charge distributions in 1,2-dinitrosoethylene and furoxan. 2. *Ab initio* electrostatic potentials and relative bond strengths," Tetrahedron **45**, 6537 (1989).

[5]E. Sedano, C. Sarasola, J. M. Ugalde, I. X. Irazabalbeitia, and A. G. Guerrero, "Conformations and charge distributions in 1,2-dinitrosoethylene and furoxan. 1. An *ab initio* molecular orbital study," J. Phys. Chem. **92**, 5094 (1988).

[6]K.-J. Hwang, I. Jo, Y. Ah Shin, S. Yoo, and J. H. Lee, "Furoxans as potential nitric oxide generator: Mechanistic speculation on the electron impacted fragmentation," Tetrahedron Lett. **36**, 3337 (1995).

[7]S. G. Zlotin, A. M. Churakov, O. A. Luk'yanov, N. N. Makhova, A. Yu. Sukhorukov, and A. Tartakovsky, "Novel approaches to pharmacology-oriented and energy rich organic nitrogen-oxygen systems," Mendeleev Commun. **25**, 399 (2015).

[8]L. L. Fershtat, I. V. Ananyev, and N. N. Makhova, "Efficient assembly of mono- and bis(1,2,4-oxadiazol-3-yl)furoxan scaffolds via tandem reactions of furoxanylamidoximes," RSC Adv. **5**, 47248 (2015).

[9]C. O. Kim, J. W. Jung, M. Kim, T.-H. Kang, K. Ihm, K.-J. Kim, B. Kim, J. W. Park, H.-W. Nam, and K.-J. Hwang, "Low energy electron beam irradiation promoted selective cleavage of surface furoxan," Langmuir **19**, 4504 (2003).

[10]D. Fischer, T. M. Klapotke, and J. Stierstorfer, "Synthesis and characterization of diaminobisfuroxane," Eur. J. Inorg. Chem. **2014**, 5808–5811.

[11]R. V. Tsyshevsky and M. M. Kuklja, "Decomposition mechanisms and kinetics of novel energetic molecules BNFF-1 and ANFF-1: Quantum-chemical modeling," Molecules **18**, 8500 (2013).

[12]D. Yaempongsa, "Quantum chemical studies of new energetic molecules," Master thesis in physical chemistry, KTH Kemivetenskap, online version, http://www.diva-portal.se/smash/get/diva2:720739/FULLTEXT01.pdf.

[13]T. Brinck and M. Rahm, "Theoretical design of green energetic materials: Predicting stability, detection, synthesis and performance," in *Green Energetic Materials*, 1st Edition, edited by T. Brinck (John Wiley & Sons, Ltd., 2014), Chap. 2.

[14]P. Politzer, J. S. Murray, J. M. Seminario, P. Lane, M. E. Grice, and M. C. Concha, "Computational characterization of energetic materials," J. Mol. Struct.: THEOCHEM **573**, 1 (2001).

[15]P. Politzer and J. S. Murray, "Some perspectives on sensitivity to initiation of detonation," in *Green Energetic Materials*, 1st Edition, edited by T. Brinck (John Wiley & Sons, Ltd., 2014), Chap. 3.

[16]M. Miao, Z. A. Dreger, J. E. Patterson, and Y. M. Gupta, "Shock wave induced decomposition of RDX: Quantum chemistry calculation," J. Phys. Chem. A **112**, 7383 (2008).

[17]F. J. Owens, "Calculation of energy barriers for bond rupture in some energetic molecules," J. Mol. Struct.: THEOCHEM **370**, 11 (1996).

[18]F. M. Nareetsile, "Solid state reactions," in *Solventless Isomerisation Reactions of Six-Coordinate Complexes of Ruthenium and Molybdenum*, Ph.D. thesis, (Department of Chemistry, University of Witwatersrand, 2006), Chap. 2, online version: http://wiredspace.wits.ac.za/bitstream/handle/10539/1654/Chapter%202-%20Final.pdf?sequence=2&isAllowed=y.

[19]A. L. Ramaswamy, "Microscopic initiation mechanisms in energetic material crystals," J. Energ. Mater. **2**, 195 (2001).

[20]G. E. Hardy, J. C. Baldwin, J. I. Zink, W. C. Kaska, P.-H. Liu, and L. Dubois, "Triboluminescence spectroscopy of aromatic compounds," J. Am. Chem. Soc. **99**, 3533 (1977).

[21]J. I. Zink and W. C. Kaska, "Triboluminescence of hexaphenylcarbodiphosphorane: Emission from a molecular excited state populated by mechanical stress," J. Am. Chem. Soc. **95**, 7510 (1973).

[22]J. I. Zink, G. E. Hardy, and J. E. Sutton, "Triboluminescence of sugars," J. Phys. Chem. **80**, 248 (1976).

[23]J. I. Zink and W. Klimt, "Triboluminescence of coumarin. Fluorescence and dynamic spectral features excited by mechanical stress," J. Am. Chem. Soc. **96**, 4690 (1974).

[24]W. Beese and J. I. Zink, "Intensity of triboluminescence," J. Lumin. **29**, 119 (1984).

[25]G. E. Hardy and J. I. Zink, "Triboluminescence and pressure dependence of the photoluminescence of tetrahedral manganese (II) Complexes," Inorg. Chem. **15**, 3061 (1976).

[26]S. H. Lin, D. Wutz, Z. Z. Ho, and H. Eyring, "Mechanisms of triboluminescence," Proc. Natl. Acad. Sci. U. S. A. **77**, 1245 (1980).

[27]A. Bhattacharya, Y. Q. Guo, and E. R. Bernstein, "Nonadiabatic reactions of energetic molecules," Acc. Chem. Res. **43**, 1476 (2010).

[28]Y. Q. Guo, A. Bhattacharya, and E. R. Bernstein, "Decomposition of nitramine energetic materials in excited electronic states: RDX and HMX," J. Chem. Phys. **122**, 244310 (2005).

[29]Y. Q. Guo, M. Greenfield, A. Bhattacharya, and E. R. Bernstein, "On the excited electronic state dissociation of nitramine energetic materials and model systems," J. Chem. Phys. **127**, 154301 (2007).

[30]M. M. Kuklja, "Role of electronic excitations in explosive decomposition of solids," J. Appl. Phys. **89**, 4156 (2001).

[31]E. J. Reed, J. D. Joannopoulos, and L. E. Fried, "Electronic excitations in shocked nitromethane," Phys. Rev. B **62**, 16500 (2000).

[32]K. Takatsuka, T. Yonehara, K. Hanasaki, and Y. Arasaki, *Chemical Theory Beyond the Born-Oppenheimer Paradigm: Nonadiabatic Electronic and Nuclear Dynamics in Chemical Reactions* (World Scientific Publishing Co. Pte. Ltd., Singapore, 2015).

[33]B. O. Roos, "Theoretical studies of electronically excited states of molecular systems using multiconfigurational perturbation theory," Acc. Chem. Res. **32**, 137 (1999).

[34]P. Pulay, "A perspective on the CASPT2 method," Int. J. Quantum Chem. **111**, 3273 (2011).

[35]P. Celani and H.-J. Werner, "Multireference perturbation theory for large restricted and selected active space reference wave functions," J. Chem. Phys. **112**, 5546 (2000).

[36]C. J. S. M. Simpson, P. T. Griffiths, H. L. Wallaart, and M. Towrie, "Photodissociation of alkyl nitrites adsorbed on an MgF_2 surface. Rotational and translational energy distributions of product $NO(\nu, J)$ molecules," Chem. Phys. Lett. **263**, 19 (1996).

[37]A. Bhattacharya and E. R. Bernstein, "Nonadiabatic decomposition of gas-phase RDX through conical Intersections: An ONIOM-CASSCF study," J. Phys. Chem. A **115**, 4135 (2011).

[38]B. Yuan, Z. Yu, and E. R. Bernstein, "Initial mechanisms for the decomposition of electronically excited energetic salts: TKX-50 and MAD-x1," J. Phys. Chem. A **119**, 2965 (2015).

[39]B. Yuan, Z. Yu, and E. R. Bernstein, "Azole energetic materials: Initial mechanisms for the energy release from electronical excited nitropyrazoles," J. Chem. Phys. **140**, 034320 (2014).

[40]B. Yuan, Z. Yu, and E. R. Bernstein, "Initial decomposition mechanism for the energy release from electronically excited energetic materials: FOX-7 (1,1-diamino-2,2-dinitroethene, $C_2H_4N_4O_4$)," J. Chem. Phys. **140**, 074708 (2014).

[41]Z. Yu and E. R. Bernstein, "Decomposition of pentaerythritoltetranitrate [$C(CH_2ONO_2)_4$] following electronic excitation," J. Chem. Phys. **135**, 154305 (2011).

[42]Z. Yu and E. R. Bernstein, "Experimental and theoretical studies of the decomposition of new imidazole based energetic materials: Model systems," J. Chem. Phys. **137**, 114303 (2012).

[43]Z. Yu and E. R. Bernstein, "On the decomposition mechanisms of new imidazole-based energetic materials," J. Phys. Chem. **117**, 1756 (2013).

[44]A. Bhattacharya, Y. Q. Guo, and E. R. Bernstein, "Experimental and theoretical exploration of the initial steps in the decomposition of a model nitramine energetic material: Dimethylnitramine," J. Phys. Chem. A **113**, 811 (2009).

[45]N. Fischer, D. Izsak, T. M. Klapotke, S. Rappengluck, and J. Stierstorfer, "Nitrogen-rich 5,5′-bistetrazolates and their potential use in propellant systems: A comprehensive study," Chem. Eur. J. **18**, 4051 (2012).

[46]B. O. Roos, K. Andersson, and M. P. Fulscher, "Towards an accurate molecular orbital theory for excited states: The benzene molecule," Chem. Phys. Lett. **192**, 5 (1992).

[47]L. Streit, F. B. C. Machado, and R. Custodio, "Double ionization energies of HCl, HBr, Cl_2 and Br_2 molecules: An MRCI study," Chem. Phys. Lett. **506**, 22 (2011).

[48]A. T. Rhys Williams, *An Introduction to Fluorescence Spectroscopy* (PerkinElmer, Inc., 1981), http://www.chem.uci.edu/~dmitryf/manuals/Fundamentals/Fluorescence%20Spectroscopy.pdf.